Effect of clay content and distribution on hydraulic and geophysical properties of synthetic sand-clay mixtures

Gordon Osterman: Department of Earth and Environmental Science, Rutgers University-Newark, Newark, NJ, USA; gko4@rutgers.edu (corresponding author)

Madhuri Sugand: Lancaster Environment Centre, Lancaster University, Lancaster, UK, Currently at the REACH Centre, Lancaster University, Lancaster, UK; madhurisugand@outlook.com

Kristina Keating: Department of Earth and Environmental Science, Rutgers University-Newark, Newark, NJ, USA; kmkeat@newark.rutgers.edu

Andrew Binley: Lancaster Environment Centre, Lancaster University, Lancaster, UK; a.binley@lancaster.ac.uk

Lee Slater: Department of Earth and Environmental Science, Rutgers University-Newark, Newark, NJ, USA: lslater@newark.rutgers.edu

ABSTRACT

Geophysical methods show promise for detecting the spatial variability of subsurface clay content and its effect on subsurface hydraulic properties. We present a laboratory study that examines the influence of clay content and distribution on the relationships between hydraulic conductivity, *K*, and the physical and geophysical properties of the media. Two geophysical methods are investigated: spectral induced polarization (SIP) and nuclear magnetic resonance (NMR). We used synthetic sediment mixtures of sand and up to 10% kaolinite clay by mass; the clay was homogenously mixed or was present as large (~5 mm) clusters distributed through the sample. *K* varies moderately well (normalized root-mean square error, *NRMSE* = 0.393) with the pore-volume normalized surface area, S_{por}, a proxy measure of clay content, in the homogenous samples and poorly (*NRMSE* = 0.507) when the clustered samples are included in the fit. SIP parameters show moderately good to excellent fits with S_{por} for homogeneous samples (*NRMSE*=0.0783 to 0.139) and moderately good to good fits for clustered samples (*NMRSE*=0.140 to 0.336) and the coefficients describing the polarizability of the samples depend on clay distribution. NMR parameters vary moderately well with S_{por} in the homogeneous samples (*NMRSE*=0.341 to 0.412) and poorly (NRMSE=1.08 to 6.04) in the clustered samples. SIP parameters vary moderately well with *K* (*NRMSE*=0.301 to 0.466), however, the relationship between the SIP parameters and *K* is compromised by the non-negligible polarization of the clay clusters. NMR parameters show good to excellent fits with *K* (*NRMSE*=0.0789 to 0.116). For both SIP and NMR, fitting homogeneous and clustered samples together does not compromise the fit quality. These results suggest that the geophysical measurements are better predictors of *K* in heterogeneous porous media than bulk measures of pore geometry such as S_{por}.

INTRODUCTION

Accurate hydrogeological models require that the distribution of hydraulic properties in the system is well-quantified. Typically, the hydrogeology is characterized using aquifer tests performed in boreholes drilled into the groundwater system. In heterogeneous aquifers, a sparse network of wells may not accurately resolve the spatial variation in hydraulic properties. Of particular interest are the quantity and distribution of clay minerals throughout the subsurface, which are known to have a disproportionate impact on subsurface hydraulic properties, particularly hydraulic conductivity (Neuzil, 1986; Keller et al., 1989).

Geophysical methods offer relatively fast and easy means of assessing spatial variations in the physical and hydraulic properties of the subsurface (see e.g. Binley et al., 2015) and have been used to map clay in the subsurface for decades (e.g. Palacky, 1987). Two relatively new methods in groundwater geophysics, spectral induced polarization (SIP) and nuclear magnetic resonance (NMR), are sensitive to the physical properties of porous media that control fluid flow (Weller et al., 2010; Minagawa et al., 2008), allowing researchers to develop petrophysical models using SIP and NMR parameters to estimate hydraulic conductivity (Börner et al., 1996; Revil et al., 2015; Seevers, 1966; Dlubac et al., 2013; Osterman et al., 2016). Furthermore, studies have shown that SIP and NMR signals are sensitive to variations in clay content (e.g. Vinegar and Waxman, 1984; Okay et al., 2014; Costabel and Yaramanci, 2013).

Clay distribution is known to control electrical measurements in synthetic sediments. Wildenschild et al. (2000) tested the effect of montmorillonite distribution on electrical conductivity measurements, hydraulic conductivity, and the hydraulic radius estimated using the approach of Revil and Cathles (1999). They found that surface conduction decreased when the clay was clustered as opposed to homogeneously distributed. Sugand (2015) extended the approach of Wildenschild et al. (2000) to study the impact of clay distribution on SIP measurements and SIP-hydraulic conductivity models. They found that while the SIP measurements were sensitive to the distribution of clay, the tested SIP-hydraulic conductivity models from the literature (Revil 2012; Weller et al., 2015a) performed well regardless of clay distribution. However, their work did not include direct measurements of the pore geometry of their samples.

Previous studies have examined the effect clay heterogeneity on the NMR response of water-saturated sediments. Anand et al., (2006) found that increasing the kaolinite or bentonite content within homogeneous sand-clay mixtures resulted in a shift in the NMR relaxation time distribution to shorter relaxation times. However, increasing the clay content when distributed as a laminated surface within a sand matrix caused a second, short relaxation time peak to appear. In clay-bearing natural soils, Stingaciu et al. (2009) found that NMR relaxation time distributions compared well with pore size distributions measured from mercury injection and water retention curves. However, the authors found that the surface area normalized by pore volume did not correspond to the pore geometry detected by the NMR measurements. The effect of heterogeneous pore size distributions on NMR in unconsolidated materials has been studied in microporous silica beads (Hinedi et al. 1997) and in zeolites (Swanson et al., 2015). In both cases, the bimodal pore size distributions were reflected in the NMR relaxation time distributions. However, Hinedi et al. (1997) found that the surface area normalized by pore volume was dominantly controlled by the microporosity whereas the NMR measurements were more sensitive to the intergranular pores. While these previous studies have examined the effect of clay heterogeneity on the NMR response, they did not explore how the clay distribution impacted the link between the NMR parameters and the hydraulic properties of the sediments.

In this laboratory study, we extend the work of Wildenschild et al. (2000), Anand et al. (2006), and Sugand (2015) by posing the following research question: what are the impacts of clay content and clay distribution in synthetic sand-clay mixtures on the petrophysical links between geophysical (SIP and NMR) parameters and the measured physical and hydraulic parameters? We mix clean, silica sand with up to 10% of kaolinite clay by mass and distribute the clay either homogeneously or as large (~5 mm in diameter), randomly dispersed clay clusters. The clay clusters are proxies for the heterogeneous clay distributions in natural sediments such as thin sand lenses; although they are imperfect reflections of natural sediments, they provide a strong contrast to compare homogenous clay distributions against. The results from this study represent a step towards understanding how the distribution of clay in unconsolidated sediments impacts measured geophysical parameters and petrophysical models.

THEORY

Hydraulic conductivity

Hydraulic conductivity (*K*, units of m/s), is defined in Darcy's Law as the proportionality constant linking the rate of fluid flow to the hydraulic head gradient across a porous medium and quantifies the ability of a porous medium to conduct fluid flow. For unconsolidated samples, *K* is typically measured directly in the laboratory using one of two Darcy flow experiments: a constant head or a falling head experiment (Domenico and Schwartz, 1990). Alternatively, *K* can be estimated from characteristic physical properties of the porous medium; combining Darcy's Law with the Hagen-Poiseuille Law shows that *K* is proportional to the square of a characteristic pore size (Bear, 1972). Johnson et al. (1987) rigorously defined this length scale as the dynamically interconnected hydraulic radius, which we refer to simply as the hydraulic radius.

However, it is difficult to measure the hydraulic radius directly, especially in unconsolidated sediments, so researchers have explored using proxy measures of hydraulic radius to estimate *K*.

An alternate pore geometry used for estimating hydraulic conductivity is the pore-volume normalized surface area (S_{por}, units of 1/µm), which is often considered to be inversely proportional to the hydraulic radius. S_{por} can be calculated from,

$$S_{por}=S_{SA}\rho_g\frac{1-\phi}{\phi}, \tag{1}$$

where S_{SA} is the specific surface area (m^2/g), ϕ is the porosity (-), and ρ_g is the matrix density (g/m^2). Clay has a much higher S_{SA} than sand and in unconsolidated sand-clay mixtures with a single type of sand and clay S_{por} is a rough proxy for the clay content with high S_{por} values indicating high clay content.

Estimating *K* from S_{por} can be done using the Kozeny-Carman capillary bundle model of the form (Carman, 1939),

$$K=A_{KC}\phi S_{por}^{-2}, \tag{2}$$

where A_{KC} is a fitting coefficient that accounts for the tortuosity of the pore space and varies based on the soil texture (Chapuis and Aubertin, 2003). Ozgumus et al. (2014) compiled a set of A_{KC} values from numerous computational and experimental studies ranging between 4–14×10^{-5} m/µm^2/s. Although the exponent in equation 2 is typically set to 2 (Carrier, 2003), other researchers have suggested alternative values. For instance, Pape et al. (1987) suggest a value of 3.1 based on a fractal model of the pore space.

The dependence of K on S_{por} in equation 2 suggests that increasing the clay content of a porous medium will reduce K. Chapuis and Aubertin (2003) cautioned that equation 2 only holds for clayey sediments when they are fully saturated and non-compacted. Furthermore, S_{por} is a bulk property of a porous medium and equation 2 implicitly assumes that S_{por} is homogeneous throughout the volume of interest. In heterogeneous sediments, equation 2 may not be valid.

Spectral induced polarization

SIP, which evolved from the use of induced polarization in mineral exploration, is employed for a wide range of near-surface geophysical problems, including hydraulic parameter estimation. In this section we briefly review the theory of SIP; more thorough presentations can be found in: Vinegar and Waxman (1984); Revil and Florsch (2010); Weller et al. (2010); Kemna et al. (2012); Revil (2012, 2013); Revil et al. (2017); and Weller et al. (2015a). The SIP measurement involves injecting a sinusoidal alternating electrical current into a porous medium at low frequencies (mHz to kHz) and measuring the resulting phase-delayed sinusoidal voltage. The measured complex electrical conductivity σ^* (S/m) can be decomposed into real (σ') and quadrature (σ'') components,

$$\sigma^*(f)=|\sigma|e^{i\theta(f)}=\sigma'(f)+i\sigma''(f), \tag{3}$$

$$\tan(\theta)=\frac{\sigma''(f)}{\sigma'(f)}, \tag{4}$$

where $|\sigma|$ is the magnitude of the complex conductivity, θ is the phase angle (rad), f is the injected current frequency (Hz), and i is the unit imaginary number.

The σ' component quantifies electrolytic conduction resulting from the unrestricted electromigration of ions through both the pore fluid and the electrical double layer (EDL) that forms at the fluid-mineral interface (Sen et al., 1988; Revil and Cathles, 1999),

$$\sigma'(f) = \frac{1}{F}\sigma_f + \sigma_s'. \tag{5}$$

F is Archie's electrical formation factor (Archie, 1942; Vinegar and Waxman, 1984) which is related to the tortuosity-normalized porosity, σ_f is the saturating fluid conductivity, and $\sigma_s^{'}$ is the in-phase surface conductivity at the pore interface. While F and $\sigma_s^{'}$ are functions of the pore geometry (Weller et al., 2013, Revil 2013), the parameters cannot be readily disentangled from σ_f, which makes σ' a non-ideal parameter for petrophysical relationships (Slater, 2007). The σ'' component represents restricted electromigration, which results in a reversible build-up of ions, or polarization, throughout the pore space. In saturated geological media composed of insulating grains, ionic polarization is thought to be caused by two dominant mechanisms in the 0.01-100 Hz range: EDL polarization (Leroy et al., 2008; Revil, 2012; Revil, 2013, Revil et al., 2017) and membrane polarization (Marshall and Madden, 1959; Titov et al., 2002). Both mechanisms are strongly dependent on grain and pore geometry (Revil and Florsch, 2010; Bücker and Hördt, 2013) and relatively insensitive to σ_f (Weller et al., 2011).

A single, characteristic value of σ'' is often used to represent an entire SIP spectrum and σ'' at 1 Hz $\left(\sigma_{1Hz}^{''}\right)$ is commonly chosen as it is a frequency readily measurable using laboratory, borehole, and field SIP equipment. Weller et al. (2010) compiled SIP data on homogeneously mixed sand and sand-clay sediments from Slater and Glaser (2003) and Slater et al. (2006), which showed an approximately linear relationship between $\sigma_{1Hz}^{''}$ and S_{por}. Revil et al. (2017)

extend on this relationship and developed a model of electrical conduction in soils where σ''_{1Hz} is approximated by S_{por} as,

$$\sigma''_{1Hz} = C_s \frac{S_{por}}{F(1\text{-}\phi)}. \tag{6}$$

Here C_s = 7.36×10^{-2} mS um/m per Revil et al. (2013; 2017) (see derivation in Appendix A). Similar to the specific polarizability from Weller et al. (2010), C_s is a function of ionic density and mobility in the Stern Layer at the fluid-mineral interface and therefore a second-order function of pore fluid chemistry (Weller et al., 2011). However, the specific polarizability as defined by Weller et al. (2010) is a proportionality constant between S_{por} and σ" which, according to equation 6, suggests that the specific polarizability implicitly contains information on F and ϕ whereas C_s is independent of these parameters. Note that the units given for C_s simplify to (nS) but are reported as (mS um/m) to reflect the units of the measurements used to derive C_s.

Petrophysical information may be extracted from the entire SIP spectrum by modeling it with a phenomenological relaxation time model such as a Debye-decomposition (Nordsiek and Weller, 2008; Zisser et al., 2010). In the Debye-decomposition approach to modeling SIP spectra of Nordsiek and Weller (2008), $\sigma^*(f)$ is given by a superposition of N Debye models,

$$\sigma^*(f) = \sigma_0 \left(1\text{-} \sum_{j=1}^{N} m_j \left(1\text{-} \frac{1}{1+i2\pi f \tau_j} \right) \right)^{-1}, \tag{7}$$

$$\sum_{j=1}^{N} m_j = m_t = \frac{\sigma_\infty \text{-} \sigma_0}{\sigma_\infty}, \tag{8}$$

where m_j (unitless) and τ_j (s) are the chargeability and the SIP relaxation time parameters for the j^{th} relaxation term, m_t is the total chargeability of the pore space (Sumner, 1976), σ_∞ is the conductivity magnitude at the high frequency asymptote and σ_0 is the conductivity magnitude at zero frequency. m_t defines the relative change in the magnitude of σ^* over the frequency spectrum. The normalized chargeability (m_n, units of S/m) is calculated by scaling m_t by σ_0,

$$m_n = m_t \sigma_0. \tag{9}$$

Weller et al. (2010) found that m_n varies linearly with S_{por}, and Revil et al. (2017) gave the following expression,

$$m_n = C_m \frac{S_{por}}{F(1\text{-}\phi)}, \tag{10}$$

where C_m is similar to C_s and the specific polarizability (Weller et al., 2010). From Revil et al. (2013; 2017), $C_m = 5.96\times10^{-1}$ mS um/m (see Appendix A).

K can be estimated from SIP parameters based on power-law relationships,

$$K = \frac{A_S}{F(\sigma''_{1Hz})^2}. \tag{11}$$

$$K = \frac{A_m}{F m_n^2}. \tag{12}$$

Where As and Ap are fitting coefficients (mS^2/m/s). Equations 11 and 12 are simplified versions of the equations in Weller et al. (2015a), which were derived from 22 samples of unconsolidated sediments. In the version of equation 11 given in Weller et al., (2015a) the exponent for σ''_{1Hz} is –2.27, the exponent for F is –1.12, and $A_s = 1.19\times10^{-6}$ mS^2/m/s; in the version of equation 12 given in Weller et al. (2015a) the exponent for m_n is -2.21, the exponent for F is –1.07, and A_m $=9.55\times10^{-5}$ mS^2/m/s. Note that these values of A_s and A_m were originally defined for permeability (k) models where permeability was measured in units of m^2. For water-saturated media at 25°C, $K=V*k$, where $V=1.10\times10^7$ m*s and has been used to scale the coefficients in Weller et al. (2015a) for use here. Although the models we use are not exactly the same as those from Weller et al. (2015a), the exponents are sufficiently similar that we can compare our results to theirs.

Nuclear magnetic resonance

Geophysical applications of NMR focus on the detection of hydrogen protons in pore fluids, primarily in water and hydrocarbons, to assess their quantity and mobility. A thorough review of proton NMR for geophysical applications and hydraulic parameter estimation is provided in: Timur (1969); Banavar and Schwartz (1987); Morriss et al. (1997); Kleinberg and Horsfield (1990); Howard and Kenyon (1992); Kenyon et al. (1995); Kleinberg (1996); Godefroy et al. (2001); and Behroozmand et al. (2015). The NMR experiment consists of tipping the nuclear spins of the protons away from their equilibrium orientation with a static magnetic field using a secondary oscillating magnetic field. After terminating the secondary magnetic field, the protons relax back to their equilibrium orientation, a process that produces a measurable signal, $A(t)$ that can be modeled as a superposition of M exponential decays,

$$A(t)=A_0\sum_{j=1}^{M}h_j e^{-t/T_{2j}}, \tag{13}$$

where A_0 (arbitrary units) is the signal magnitude at time t=0; h_j (-) and T_{2j} (s) are the signal fraction and transverse relaxation time of the j^{th} portion of the signal, respectively. The A_0 is proportional to the number of protons in the pore space tipped into the transverse plane and thus gives the water content in the pore space.

The measured T_2 relaxation times arise from three parallel relaxation mechanisms,

$$T_2^{-1}=T_{2B}^{-1}+T_{2S}^{-1}+T_{2D}^{-1}, \tag{14}$$

where T_{2B} is the bulk relaxation time, which corresponds to relaxation occurring due to dipolar spin-coupling between water molecules, T_{2S} is the surface relaxation time, which corresponds to relaxation occurring due to proton-electron spin coupling at paramagnetic mineral sites at the fluid-mineral interface, and T_{2D} is the diffusion relaxation time, which quantifies the apparent relaxation that results from the dephasing of protons as they diffuse through pore-scale magnetic field inhomogeneities. As T_{2B} and T_{2D} contain little information concerning the pore geometries controlling fluid flow, it is desirable to minimize or eliminate their influence. T_{2B} has a constant value for water (~3 s) that is much slower than T_{2S} and can be subtracted with little impact on T_2 (e.g. Keating and Knight, 2007). The effect of T_{2D} can be mitigated by using a Carr-Purcell-Meiboom-Gill, or CPMG (Meiboom and Gill, 1958) pulse sequence to rephase the proton spins with very short pulse intervals, or echo times (Kleinberg and Horsfield, 1990; Anand and Hirasaki, 2008).

Brownstein and Tarr (1979) found that T_{2S} is controlled by the distance a proton travels before interacting with a pore wall, which is related to the size of the pore, as well as the density and distribution of paramagnetic impurities at the surface quantified by the surface relaxivity, ρ_2

(µm/s) (Kleinberg, 1996). If relaxation occurs in the fast diffusion regime then each pore is characterized by a single relaxation time T_{2j} and signal amplitude h_j (Brownstein and Tarr, 1979; Kleinberg and Horsfield, 1990). Assuming ρ_2 does not vary to a large degree within the observed geological media (Foley et al., 1996), the distribution of T_2 relaxation times in equation 13 may be interpreted as a proxy for the pore size distribution of a system (Kleinberg, 1996), although in certain geological environments (e.g. formations containing iron(III)-bearing minerals) this assumption may not be true (Keating and Knight, 2012).

In relatively homogeneous porous media, the entire system may be characterized by a single, characteristic relaxation rate T_{2S}^{-1}, where,

$$T_{2S}^{-1}=\rho_2 S_{por}. \tag{15}$$

The most commonly used characteristic value from the T_2 distribution is the mean-log relaxation time T_{2ml} as it incorporates information from the entire T_2 distribution. We refer to surface relaxivities derived using T_{2ml} as ρ_{2ml}. The relaxation time at the peak of the distribution, T_{2p}, has also been shown to correlate well with the hydraulic radius (Keating, 2014; Osterman et al., 2016) and to be well suited for estimating K (Dlugosch et al., 2013). Here we refer to surface relaxivities derived using T_{2p} as ρ_{2p}. Godefroy et al. (2001) found for a set of clean silicon carbide samples that ρ_2 ranged from $3 \leq \rho_2 \leq 5$ µm/s. Similarly, Kleinberg (1996) found that $\rho_2=3$ µm/s for quartz. Note that the derived value of ρ_2 depends on the characteristic T_2 value and how the pore geometry is measured. For example, Stingaciu et al. (2009) found that S_{por} was not a good pore geometry to use for estimating ρ_2 in natural, clay-bearing soils, as it did not reflect the pore space heterogeneity in their samples.

In regularized inversions commonly used to extract the relaxation time distribution from NMR data, the choice of regularization parameter can strongly impact the shape of the T_2 distribution and the location of peaks. T_{2ml} is relatively robust to variations in the regularization parameter, which makes it an appealing relaxation time to use. By contrast, T_{2p} may vary to a far greater degree as a function of the regularization parameter and caution must be exercised when interpreting T_{2p}.

Based on equation 15, K models such as the Schlumberger-Doll Research equation (SDR) have been derived for NMR measurements (Seevers, 1966; Banavar and Schwartz, 1987) with the form,

$$K = B_{ml/p} \phi_{NMR}^{n} T_2^2, \tag{16}$$

where ϕ_{NMR} is porosity estimated from the NMR signal amplitude A_0, $B_{ml/p}$ refers to the fitting coefficient where the subscript corresponds to the characteristic relaxation time used (ml for T_{2ml}, or p for T_{2p}), and n is an exponent used to describe the tortuosity of the pore space. In the NMR literature n is typically set to 4 (Kenyon et al., 1995). Maurer and Knight (2016) found that for a broad range of borehole measurements in unconsolidated sedimentary environments, B_{ml} =0.80–4.70 m/s^3 when n=4. Another model that is commonly used to estimate K is the Timur-Coates (TC); the TC model is an empirical model that uses an estimate of the irreducible water volume, determined from the NMR relaxation time distribution, to predict K (Timur, 1969; Coates et al., 1991). Other researchers have developed models for K or k that are optimized for specific geologic materials, such as unconsolidated coarse grain materials (Dlugosch et al., 2013), fine grain sediments (Daigle and Dugan, 2009), and fine-grain clay rich mudstones (Daigle and Dugan, 2011).

MATERIALS AND METHODS

To test the effect of clay content and distribution in synthetic sand-clay mixtures on the relationships between the measured physical and hydraulic parameters and the geophysical parameters, we prepared 21 synthetic mixtures with varying ratios of sand and clay and collected S_{por}, K, SIP, and NMR data on each sample. All measurements were run in 9.3 cm tall by 2.3 cm diameter cylindrical acrylic sample holders specially designed to support K, SIP and NMR measurements without disturbing or repacking the samples (see Wallace, 2015). The sand-clay mass ratios of 100-0, 99-1, 95-5, and 90-10 were used. For each clay concentration, three replicate samples were mixed to test the repeatability of the packing and saturation procedure.

Sample preparation

Measurements were conducted on mixtures of Wedron silica sand (Wedron Silica Co.) and kaolinite clay (Fisher Scientific). The Wedron sand is a medium, well sorted, round, clean sand with a narrow grain size distribution centered at 300 μm and a specific surface area S_{SA}=0.0388±0.0001 m^2/g. The kaolinite is a non-swelling, 1:1 phyllosilicate mineral with S_{SA}=11.552 ±0.0179 m^2/g.

Homogeneous samples were packed by first drying the sand and clay, then mixing according to the following ratios: 100%, 99%, 95%, and 90% sand, by mass. Figure 1 shows examples of the homogeneous and clustered samples with 10% clay prior to packing. The mixed sediments were dry-packed into the sample holders, with care taken to ensure no clay layers formed. Clay clusters were created by dampening the clay with deionized water and then forming it into ~5 mm diameter balls (Figure 1c) which were oven dried overnight, separate from the sand. To create the clustered samples, dry sand and clay clusters were alternately added to the sample holder to ensure the ratio of sand to clay was precisely known. The same sand-to-clay ratios were used for the clustered samples as the homogeneous samples. Care was taken to ensure that the clay clusters were not in contact with each other.

The following naming convention was used for all samples: The first letter refers to the sample type (H indicates homogeneously mixed and C indicates clay clusters), the following number indicates the percentage of clay (00, 01, 05, or 10), and the final letter indicates which repeat the sample is (A, B or C). For example, sample H01B refers to the second repeat of the homogeneous 1% clay samples.

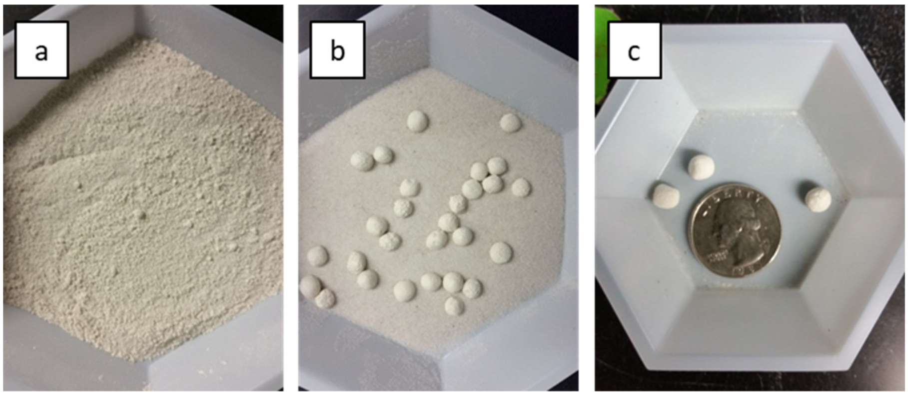

Figure 1: Examples of dry samples prior to packing, (a) 90% sand mixed homogeneously with 10% clay; (b) 90% sand mixed with 10% clay clustered in ~5 mm balls; (c) clay clusters shown with a US quarter for scale.

All samples were vacuum saturated by pulling a strong vacuum on the dry samples before flooding the sample holder with a degassed 10 mM sodium chloride brine (corresponding to a fluid conductivity of 0.11±0.01 S/m at 25°C). Electrolyte species and concentration were chosen to allow us to compare our results to other studies in the literature (e.g. Weller et al., 2010). Fluid conductivities were determined by repeatedly measuring the outflow conductivity and waiting for the fluid conductivity to stabilize. Full saturation was confirmed by comparing the known sample volume to the estimated sample volume calculated from the mass of the saturating fluid and solid matrix, using densities of 1.00 g/m^3, 2.65 g/m^3, and 2.6 g/m^3 for the saturating fluid, sand, and kaolinite.

Measurement methodologies

A constant head approach was used to measure hydraulic conductivity (see Domenico and Schwartz*,* 1990) and K was estimated from the average of four inflow-outflow head differentials. A Micromeritics ASAP 2020 surface area analyzer was used to measure S_{SA} using the Brunauer, Emmitt, and Teller, or BET, method of gas adsorption porosimetry (Brunauer et al., 1938). We used krypton as the adsorbate due to the very low surface area of the Wedron sand. Measured S_{SA} was converted to S_{por} using the porosity calculated from the mass difference between saturated and dry columns normalized by the sample volume. Although BET measurements can underestimate the surface area in clays with large inter-granular surface area (see e.g. Weller et al., 2015b), kaolinite is a 1:1 clay with limited inter-granular surface area and so BET is an acceptable method for measuring S_{SA} for the samples used in this study.

Samples for BET analysis were prepared in two ways. Homogenous samples were dried and subsampled from their columns and packed into the BET sample holders. Subsampling was not an appropriate technique for the clustered samples, so we instead recreated clustered samples specifically for BET analysis according to the exact sand-clay ratio in the sample holder.

SIP samples were run on an Ontash and Ermac PSIP instrument (Ntarlagiannis and Slater, 2014) in the frequency range from 10 mHz to 1 kHz with 5 logarithmically spaced measurements per decade. Each measurement was replicated three times to ensure repeatability. The instrument was capable of resolving phase angles as low as 0.1 mrad. In one pure sand sample and three clustered clay samples, we observed low polarization in the 0.1–10 Hz frequency range that resulted in phase angles smaller than 0.1 mrad; measurements at these frequencies were excluded from analysis. For ease of comparison with literature results, we use σ''_{1Hz} as the characteristic SIP polarization magnitude parameter. To calculate m_n, we calculated m_t-distributions and σ_0 using the Monte-Carlo Markov Chain approach of Keery et al. (2012) where random walk simulations sample a probability distribution of possible solutions.

Electrical measurements were conducted with a range of saturating fluid conductivities in order to accurately measure F (Vinegar and Waxman, 1984; Weller et al. 2013; Revil et al., 2015). All SIP parameters are calculated from measurements at low salinity, corresponding to σ_f values of approximately 0.11 S/m. For the homogeneous clay samples, high-salinity measurements were unavailable for the samples presented here. However, electrical measurements were conducted over a range of salinities corresponding to σ_f values ranging from approximately 0.11 S/m to 10 S/m on an alternate set of sand-clay mixtures packed using the same methodology, materials, and sand-clay ratios. A comparison of the S_{por}, SIP and NMR data between the data presented here and the alternate data set shows a high degree of repeatability. For each sand-clay ratio, we assign an average value of F from the same sand-clay ratio from the alternate data set. For the clustered clay samples, electrical measurements were made at two salinities (approximately 0.11 S/m and 5 S/m) and these measurements were used to calculate F.

All NMR data were collected using a 2.0 MHz Magritek Rock Core Analyzer. The CPMG pulse sequence was used with echo times of 200, 400, 800, and 1600 µs, a total measurement time of 10 s, and a recovery time of 10 s. Three cycles of 16 stacks were collected at each echo time to assess measurement repeatability. Measurements from the samples were compared using the 200 µs echo time data; longer echo times were used to assess the influence of T_{2D}. Data were inverted using a non-negative least squares algorithm with second-order Tikhonov regularization, producing a log-spaced T_2 distribution from 100 µs to 10 s (Whittall et al., 1991). The inversion regularization parameter was selected using the approach of Costabel and Yaramanci (2013) to produce the simplest model that minimizes the data misfit. Using this approach, the same regularization parameter was selected for all samples, allowing us to ignore the impact of regularization on T_{2p}. T_{2B} was determined from an average of measurements on three samples of 10 mM sodium chloride brine and found to be 2.9 s.

Characteristic T_2-relaxation times T_{2ml} and T_{2p} were used for the petrophysical analysis. To calculate T_{2ml}, we first eliminated any portion of the T_2 distribution associated with standing water in the columns, as signal associated with this water is insensitive to the hydraulic properties of the sand-clay mixtures. The effect of bulk relaxation was removed by subtracting T_{2B} from T_{2ml} and T_{2p}. Following the procedure of Keating and Knight (2007), we fit a linear regression between the square of the echo time and inverse relaxation time to demonstrate the negligible impact of T_{2D} at an echo time of 200 µs. To ensure that relaxation occurred within the fast diffusion regime, we calculated ρ_2 from equation 15 to assess whether the samples met the fast diffusion criteria, $\rho_2 R/D < 0.1$, where R (µm) is the average distance a proton travels during relaxation and D (µm^2/s) is the self-diffusion coefficient of water (Brownstein and Tarr, 1979; Ryu, 2009).

Fitting coefficients and statistics

The fitting coefficients (A_{KC} for equation 2, C_s for equation 6, C_m for equation 10, A_s for equation 11, A_m for equation 12, ρ_2 for equation 15, and B_{ml} and B_p for equation 16) were calculated as the mean-difference between log-transformed independent and dependent parameters,

$$coef = \exp\left(\frac{1}{N}\sum_{j=1}^{N}\left(\log \hat{y}_j - \log y_j\right)\right), \tag{17}$$

where *coef* refers to the fitting coefficient, N is the number of data points, $\hat{y}_j$ is the j^{th} dependent variable, and y_j is the j^{th} independent variable, which we set equal to the left-hand side of the relevant petrophysical equation or K model. To measure the quality of the fit, we calculate the normalized root mean square error (*NRMSE*) from,

$$NRMSE=\frac{1}{\log_{10}\hat{y}_{max}-\log_{10}\hat{y}_{min}}\sqrt{\frac{1}{N}\sum_{j=1}^{N}\left(\log_{10}\hat{y}_j-\log_{10}y_j\right)^2}, \tag{18}$$

where $\hat{y}_{max}$ is the maximum predicted value and $\hat{y}_{min}$ is the minimum predicted value. Since the *NRMSE* normalizes for both the number of samples as well as the data range, we can compare values of *NRMSE* between datasets. To assess the quality of the fits determined using equation 17, we use the following criteria: $NRMSE<0.1$ correspond to excellent fits, $0.1<NRMSE<0.3$, correspond to good fits, $0.3<NRMSE<0.5$ correspond to moderately good fits, while $NRMSE>0.5$ correspond to poor fits.

RESULTS

All values of K, S_{por}, ϕ, F, characteristic SIP parameters (σ''_{1Hz} and m_n), and characteristic NMR parameters used in this study are reported in Table 1. K varies from 4.98×10^{-6} m/s to 2.74×10^{-4} m/s in the homogeneous samples, but only from 1.52×10^{-4} m/s to 2.83×10^{-4} m/s in the clustered samples. S_{por} varies from 0.14 1/µm to 6.26 1/µm in the homogeneous samples and from 0.63 1/µm to 5.68 1/µm in the clustered samples. For all samples, ϕ varies from 0.36 to 0.40 with a mean of 0.38, and F varies from 4.10 to 6.26. No trend in ϕ or F is observed with increasing clay content which is likely a result of the low clay contents investigated.

Table 1*:* List of physical and geophysical parameters used for this study. Physical parameters include the hydraulic conductivity (K), the gravimetric porosity (ϕ), the pore volume normalized surface area (S_{por}), and the electrical formation factor (F). The geophysical parameters include the SIP quadrature conductivity measured at 1 Hz (σ''_{1Hz}), the SIP normalized chargeability (m_n), the NMR-estimated porosity (ϕ_{NMR}), the NMR mean-log transverse relaxation time (T_{2ml}) and the NMR transverse relaxation time at the peak of the distribution (T_{2p}).

							SIP parameters			NMR parameters		
	Clay %	Sample Name	K (m/s)	ϕ (-)	S_{por} (1/µm)	F (-)	σ'_{1Hz} (mS/m)	σ''_{1Hz} (mS/m)	m_n (mS/m)	ϕ_{NMR} (-)	T_{2ml} (s)	T_{2p} (s)
Homogeneous	0	H00A	2.74×10^{-4}	0.39	0.16	5.92 (a)	28.2	--(b)	0.028	0.37	0.584	0.604
	0	H00B	2.60×10^{-4}	0.40	0.14		29.8	0.017	0.118	0.37	0.606	0.649
	0	H00C	2.11×10^{-4}	0.37	0.18		29.3	0.004	0.058	0.38	0.498	0.562
	1	H01A	1.74×10^{-4}	0.37	0.70	5.84 (a)	28.2	0.042	0.421	0.37	0.356	0.487
	1	H01B	1.41×10^{-4}	0.39	0.61		28.7	0.027	0.343	0.38	0.322	0.422
	1	H01C	1.83×10^{-4}	0.39	0.57		28.9	0.021	0.259	0.38	0.384	0.476
	5	H05A	4.95×10^{-5}	0.36	3.03	4.24 (a)	26.5	0.074	0.947	0.39	0.191	0.316
	5	H05B	3.68×10^{-5}	0.37	2.69		28.6	0.062	0.901	0.41	0.179	0.274
	5	H05C	4.63×10^{-5}	0.37	3.03		25.5	0.079	1.139	0.40	0.199	0.340
	10	H10A	7.71×10^{-6}	0.36	5.27	5.10 (a)	26.4	0.107	1.782	0.40	0.103	0.073
	10	H10B	6.12×10^{-6}	0.38	5.39		24.8	0.124	2.293	0.41	0.102	0.062
	10	H10C	4.98×10^{-6}	0.37	6.26		24.1	0.092	1.812	0.36	0.096	0.070

Clustered	1	C01A	2.83×10^{-4}	0.38	0.63	4.62	28.3	0.009	0.056	0.37	0.566	0.649
	1	C01B	2.56×10^{-4}	0.39	0.68	4.78	30.0	--[b]	0.030	0.38	0.614	0.698
	1	C01C	2.17×10^{-4}	0.39	0.68	4.59	29.9	--[b]	0.059	0.39	0.592	0.649
	5	C05A	2.06×10^{-4}	0.38	2.99	4.51	29.8	--[b]	0.320	0.37	0.426	0.649
	5	C05B	2.12×10^{-4}	0.38	2.96	4.76	37.4	0.037	0.596	0.36	0.448	0.649
	5	C05C	2.41×10^{-4}	0.39	2.83	4.54	28.9	0.015	0.257	0.39	0.458	0.649
	10	C10A	2.21×10^{-4}	0.39	5.68	4.61	30.9	0.012	0.364	0.37	0.361	0.698
	10	C10B	1.52×10^{-4}	0.39	5.30	4.27	29.8	0.062	0.441	0.38	0.332	0.604
	10	C10C	1.80×10^{-4}	0.39	4.79	4.37	31.6	0.039	0.669	0.37	0.362	0.698

[a] Approximated *F* values from identically prepared samples with similar physical and geophysical properties.
[b] Measured phase angle below instrument resolution limit (<0.1 mrad)

K vs S_{por}

Figure 2 shows *K* plotted against ϕS_{por}^{-2} for all samples. For the data from the homogeneous samples, the fits are moderately good (A_{KC} = 1.96×10^{-4} m/μm^2/s and *NRMSE* = 0.393, see Table 2). The misfit largely results from the 0% clay samples; removing the 0% clay improves the fit (A_{KC} = 4.46×10^{-4} m/μm^2/s and *NRMSE* = 0.22). This shows that the Kozeny-Carman model (equation 2) effectively models the homogenous sample data for samples with ≥1% clay by mass; however, at low clay contents (<1% by mass), the clay may still have a large impact on the surface area but little to no impact on the hydraulic radius controlling *K*. When considering the data from both the homogeneous and clustered samples, we find that the model fits the data poorly (A_{KC} = 5.96×10^{-4} m/μm^2/s and *NRMSE* = 0.507, see Table 2) as the model is not designed for highly heterogeneous samples. The values of A_{KC} calculated for the homogeneous samples and for all the samples are larger than the values given in Ozgumus et al. (2014) of 4–14×10^{-5} m/μm^2/s, which were compiled from a number of different studies. Thus, it appears that the samples from this study have lower tortuosity than the samples analyzed in the studies reported in Ozgumus et al. (2014).

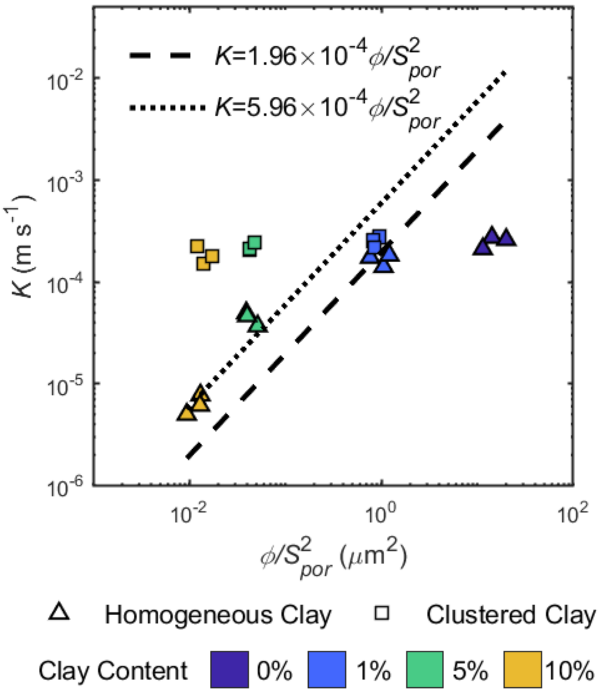

Figure 2: K versus ϕ/S_{por}^2 for all samples. The dashed line and dotted lines show the fit of Equation 2 to the homogeneous data and the entire dataset, respectively. The coefficients, (A_{KC}), and normalized root mean squared values are given in Table 2.

Table 2: Fitting coefficients and associated normalized root mean squared error (*NRMSE*) values from for the Kozeny-Carman K model (equation 2) shown in Figure 2. The coefficients for the models are given for fits to the data from the homogeneous samples and for the fits to the data from all samples. Units for the literature values were converted to the units of the fitting coefficients.

Coefficients	Homogeneous Clay Samples	All Samples	Literature Values	Units	Equation	Figure

	Value	*NRMSE*	Value	*NRMSE*				
A_{KC}	1.96×10^{-4}	0.393	5.96×10^{-4}	0.507	$4–14\times10^{-5}$ (a)	m/μm^2/s	2	1

[a] Ozgumus et al. (2014); range of coefficients were compiled from sources cited within.

Geophysical Results

Figure 3 shows SIP spectra for representative homogeneous and clustered samples over the full range of clay content. Figures 3a and 3c shows *σ'* and *σ"* spectra, respectively, for H00A, H01A, H05A, and H10A, and Figures 3b and 3d shows *σ'* and *σ"* spectra, respectively, for H00A, C01A, C05A, and C10A. Overall, we do not observe any strong or consistent trends with increasing clay content on *σ'* for homogeneous or clustered clay samples and clay distribution does not appear to have a strong impact on *σ'* in the range of clay content tested. Increasing the homogeneous clay content causes an increase in *σ"* over the entire frequency spectrum, especially at frequencies above 100 Hz (Figure 3c), as expected from the literature (Okay et al., 2014). There is little increase in *σ"* with increasing clustered clay content (Figure 3d) in the intermediate frequency range (0.1 to 10 Hz), contrasting with the behavior seen for the homogeneous samples and suggesting that *σ"* is sensitive to clay distribution. At the low frequency range, we observe an increase in *σ"* with increasing clay content that is robust across replicate samples.

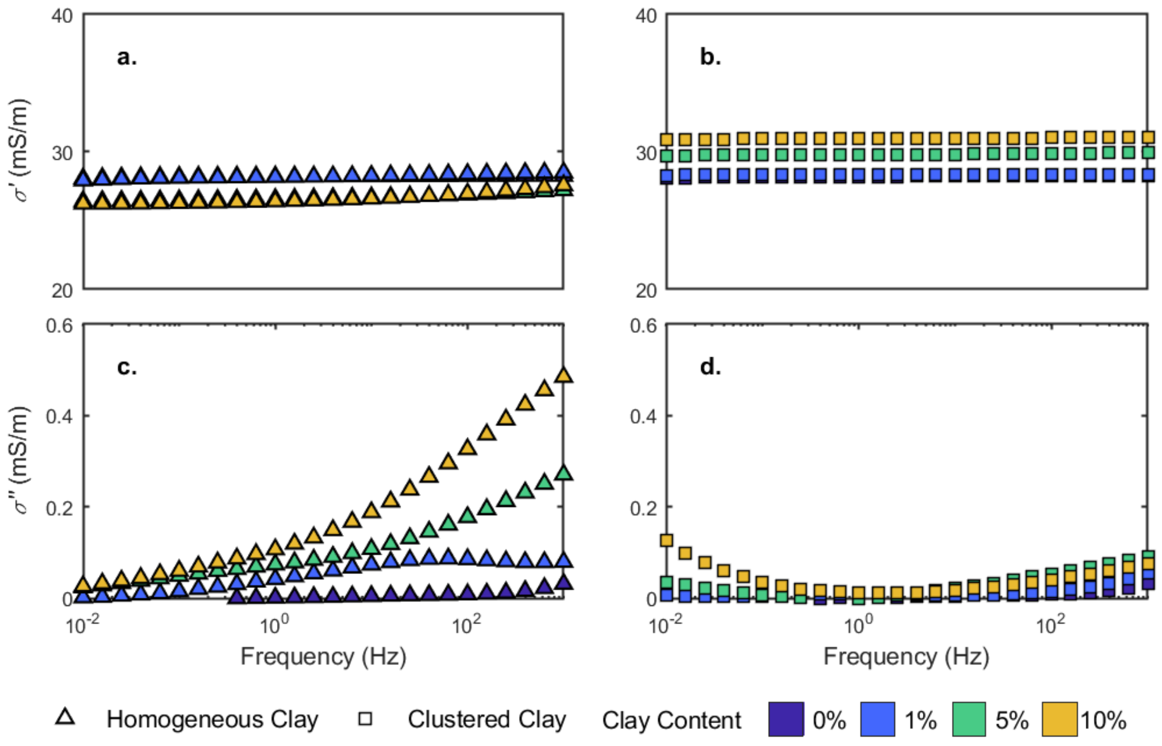

Figure 3: SIP data collected for representative homogeneous and clustered samples for each clay content (samples H00A, H01A, H05A, and H10A shown in (a) and (c); samples H00A C01A, C05A, and C10A shown in (b) and (d)). SIP σ' spectra for (a) homogeneous samples and (b) clustered samples and SIP σ" spectra for (c) homogeneous samples and (d) clustered samples.

Figure 4 shows representative NMR T_2 distributions for the homogeneous and clustered samples over the entire range of clay content. Figure 4a shows T_2 distributions for samples H00A, H01A, H05A, and H10A, and Figure 4b shows T_2 distributions for samples H00A, C01A, C05A, and C10A. Increasing homogeneous clay content decreases the average pore size which results in a shift in the dominantly mono-modal T_2 distribution from long to shorter relaxation times (Figure 4a). Similar results were shown by Anand et al. (2006) for homogeneous sand-kaolinite mixtures and by Moss and Jing (2001) for homogeneous sand-montmorillonite and sand-illite. In the clustered samples, increasing clay content results in the growth of a second, short-relaxation time peak and a small decrease in the amplitude of the original peak (Figure 4b). In the bimodal distribution, the long T_2 peaks correspond to the large, sand-bound pores, and the short T_2 peaks correspond to the small, clay-bound pores. These results match well with the T_2 distributions from the bimodal sediments studied in Anand et al. (2006) and the natural soils studied by Stingaciu et al. (2009).

We note that, for the pure sand samples, relaxation was not entirely in the fast diffusion regime ($0.09 \leq \kappa \leq 1.25$) and so the second, short-relaxation time peak observed may represent a second relaxation mode. This raises the possibility that some the signal in the shorter relaxation times for the clustered samples may also represent faster relaxation modes in the pure-sand portions of the sample in addition to the clay-bound water. For all other homogeneous samples, $\kappa < 0.1$.

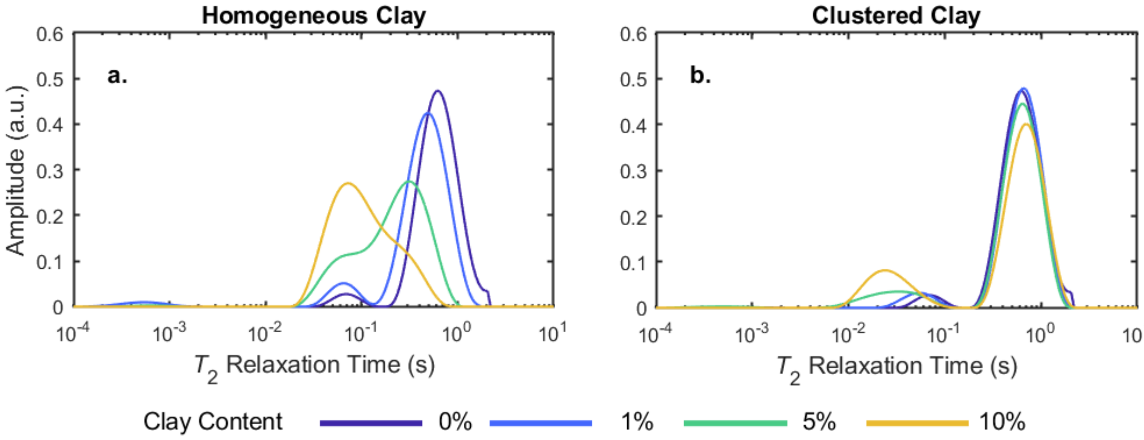

Figure 4: NMR T_2 distributions for representative (a) homogenous samples and (b) clustered samples from each clay content (samples H00A, H01A, H05A, and H10A shown in (a); samples H00A C01A, C05A, and C10A shown in (b).

Geophysical Parameters vs S_{por}

Figure 5 shows characteristic geophysical parameters plotted versus pore geometric parameters ($S_{por}/[F(1-\phi)]$ in 5a and b, S_{por} in 5c and d). Here we compare the impact of clay distribution on the relationship between the geophysical parameters and pore geometry by calcuating fitting coefficients for the homogeneous and clustered sample data separately. All coefficents and *NRMSE* values for each fit are given in Table 3.

For the relationship between $S_{por}/[F(1-\phi)]$ and $\sigma''_{1\mathrm{Hz}}$ (Figure 5a), we find a good fit for the data from the homogeneous samples ($C_s = 1.02\times10^{-1}$ mS um/m and *NRMSE*=0.139) and a moderate fit for the data from the clustered samples ($C_s = 2.15\times10^{-2}$ mS um/m and *NRMSE*=0.336). When we examine the relationship between $S_{por}/[F(1-\phi)]$ and m_n (Figure 5b), we find there is an excellent fit for the data from the homogeneous samples ($C_m = 1.27$ mS um/m and *NRMSE*=0.0783) and a good fit for the data from the clustered samples ($C_m = 0.259$ mS um/m and *NRMSE*=0.140). The fitting coefficients, C_s and C_m, for the data from the homogeneous samples are up to two times higher than values calculated from the literature; in contrast, the fitted coefficients for the clustered data are slightly lower than values given in the literature ($C_s = 7.36\times10^{-2}$ and $C_m = 5.96\times10^{-1}$ mS um/m from Revil et al., 2013; and Revil et al., 2017). This indicates that the values of the C_s and C_m presented here represent endmember values, where the high values correspond to homogeneous sand-clay media while the low values correspond to heterogeneous media.

Considering the relationship between S_{por} and $1/T_{2ml}$ (Figure 5c), we find that there is a moderately good fit for the data from the homogeneous samples (ρ_{2ml}=3.57 m/s and *NRMSE*=0.412) and a poor fit for the data from the clustered sample (ρ_{2ml}=1.02 m/s and *NRMSE*=1.08). Next when we consider the relationship between S_{por} and $1/T_{2p}$ (Figure 5d), we find there is a moderately good fit for the data from the homogeneous (ρ_{2p}=3.20 m/s and *NRMSE*=0.341), and a very poor fit for the data from the clustered samples (ρ_{2p}=6.99×10^{-1} m/s and *NRMSE*=6.04). The values of ρ_{2ml} and ρ_{2p} for the data from the homogeneous samples are within the range reported in the literature for clean quartz samples and clean silicon carbide samples (ρ_2=3–5 μm/s, Kleinberg, 1996; Godefroy et al. 2001). Although the literature values of ρ_2 were calculated using T_{2ml}, we use them as an approximation of ρ_{2p}.

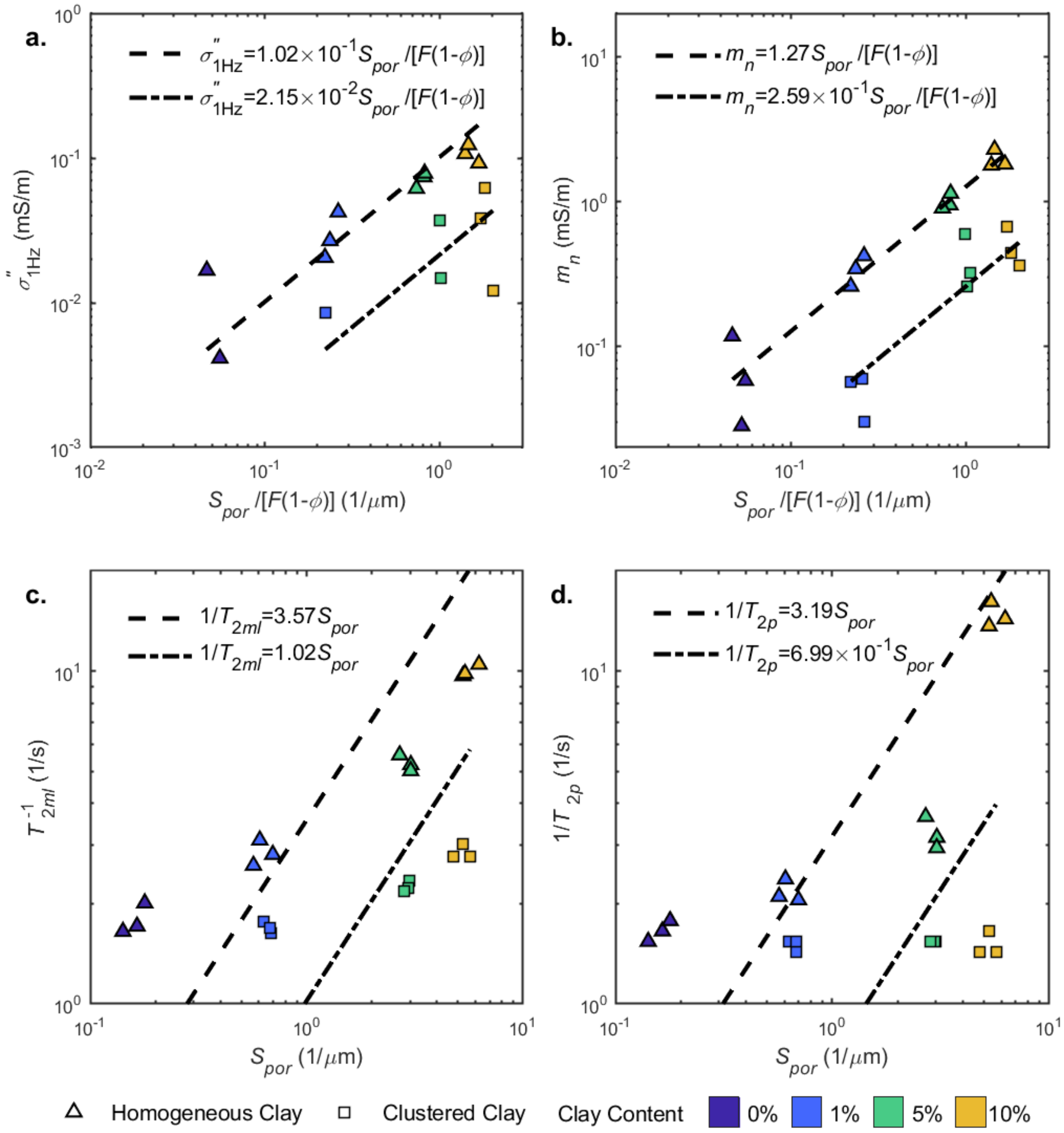

Figure 5: Characteristic geophysical parameters plotted versus pore geometric parameters: SIP parameters σ''_{1Hz} (a) and m_n (b) versus $S_{por}/[F(1-\phi)]$; NMR parameters $1/T_{2ml}$ (c) and $1/T_{2p}$ (d) versus S_{por}. The dashed line shows the line of best fit for the data from the homogeneous samples; the dot-dashed lines shows the line of best fit for the clustered samples, given by (a)

equation 6, (b) equation 10, and (c-d) equation 15. The coefficients C_s (a), C_m (b), ρ_{2ml} (c), and ρ_{2p} (d) were determined from fitting the $\log_{10}$ parameters in a least-squared sense and are given along with the corresponding normalized root mean squared values in Table 3.

Table 3: Fitting coefficients and associated normalized root mean squared error (*NRMSE*) values for the petrophysical models given in Figure 5. Coefficients from the data from the homogeneous samples are given separately from the coefficients determined from the data from the clustered samples; the fits are shown as dashed lines and dot-dashed lines in Figure 5, respectively. Note that the units listed are taken directly from the fits, and that the literature values have all been converted to these units where necessary.

	Homogeneous Clay Samples		Clustered Clay Samples					
Coefficient	Value	*NRMSE*	Value	*NRMSE*	Literature Values	Units	Equation	Figure
C_s	1.02×10^{-1}	0.139	2.15×10^{-2}	0.336	7.36×10^{-2} (a)	mS um/m	6	5a
C_m	1.27	0.0783	2.59×10^{-1}	0.140	5.96×10^{-1} (a)	mS um/m	10	5b
ρ_{2ml}	3.57	0.412	1.02	1.08	3–5 (b)	µm/s	15	5c
ρ_{2p}	3.20	0.341	6.99×10^{-1}	6.04	3–5 (b)	µm/s	15	5d

[a] Values derived from coefficients given in Revil et al. (2013) and Revil et al., (2017).

[b] Godefroy et al. (2001); Kleinberg (1996); values given for silicon carbide and, at the low end, quartz sand.

Geophysical Parameters vs *K*

Figure 6 shows *K* plotted versus characteristic geophysical parameters. The plot of *K* versus $1/\left[F\left(\sigma''_{1\mathrm{Hz}}\right)^{2}\right]$ (Figure 6a) yields a moderately good fit for the data from the homogeneous samples (A_s =4.60×10^{-7} mS^2/m/s with *NRMSE*=0.301) as well as for the entire data set (A_s =4.76×10^{-7} mS^2/m/s with *NRMSE*=0.301). We do not fit the clustered samples alone in Figure 6 alone as they do not demonstrate enough variation in *K* to extract meaningful statistics. When we consider the relationship between *K* and $1/[Fm_n^2]$ (Figure 6b) we observe moderately good fits for the homogeneous sample data (A_m =5.81×10^{-5} mS^2/m/s with *NRMSE*=0.424) and for the entire dataset (A_m =4.93×10^{-5} mS^2/m/s with *NRMSE*=0.466). We observe that both fitting coefficients A_s and A_m are remarkably consistent when fit to either the data from the homogeneous samples or to data from both the homogeneous and clustered samples. All the coefficients determined here are roughly half of the values from the literature (A_s =1.19×10^{-6} mS^2/m/s and A_m =9.55×10^{-5} mS^2/m/s, from Weller et al., 2010; Weller et al., 2015a). At high *K* (>10^{-4} m/s), we observe high variability in the SIP parameters but little variation in *K*; these values correspond to measurements collected on the pure sand and the clustered clay samples, so this observation likely occurs because the SIP measurements on these samples are nearing the instrument resolution. At lower *K* values, the SIP parameters vary more closely with *K;* recalculating fits for the homogeneous samples excluding the 0% clay samples yields good fits (A_s =6.74×10^{-7} mS^2/m/s with *NRMSE*=0.181, and A_m =1.40×10^{-4} mS^2/m/s with *NRMSE*=0.159) with fitted coefficients that are closer to the literature coefficents.

When plotting *K* versus $\phi_{NMR}^4 T_{2ml}^2$ (Figure 6c), we find there are excellent fits for the data from the homogeneous samples (B_{ml} =4.35×10^{-2} m/s^3 with *NRMSE*=0.0790) and for the combined dataset (B_{ml} =4.71×10^{-2} m/s^3 with *NRMSE*=0.0807). When we plot *K* versus $\phi_{NMR}^4 T_{2p}^2$ (Figure 6d), we observe good fits for both the data from the homogeneous samples (B_p =3.49×10^{-2} m/s^3 and *NRMSE*=0.116) and for the combined dataset (B_p =3.00×10^{-2} m/s^3 with *NRMSE*=0.104). The good-to-excellent fits derived for both the NMR parameters when using the entire dataset result from the clustered clay samples all grouping near the high-*K* limit of the homogeneous samples. This grouping is expected from the T_2-distributions (Figure 4) where there is little variation in dominant mode of the T_2 distribution as clay content increases. The values of B_{ml} and B_p determined here are substantially lower, by over an order of magnitude, than the value found in the literature of B_{ml} =0.8–4.70 m/s^3 (Maurer and Knight, 2016). This difference likely arises due to mineralogical differences between the silica-kaolinite samples studied here and the aquifer material studied in Maurer and Knight (2016).

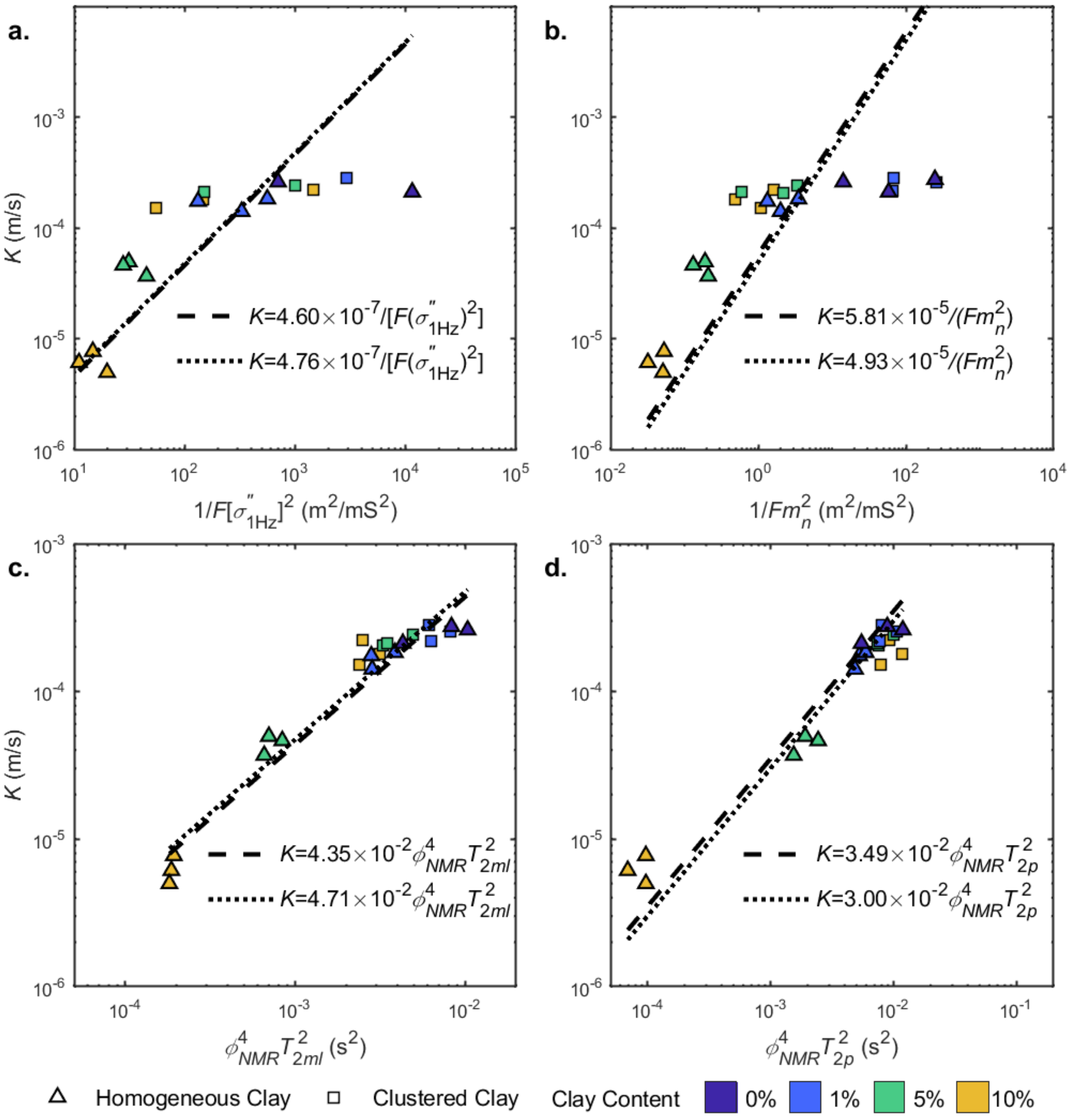

Figure 6: Geophysical parameters plotted against K: SIP parameters $1/F\left[\sigma''_{1\mathrm{Hz}}\right]^2$ (a) and $1/F\,m_n^2$ (b); NMR parameters $\phi^4_{NMR}T^2_{2ml}$ (c) and $\phi^4_{NMR}T^2_{2p}$ (d). The dashed line and dotted lines show fitted

K-models for the homogeneous data and the entire dataset, respectively, given by (a) equation 11, (b) equation 12, and (c-d) equation 16. The coefficients ((a) A_s, (b) A_m, (c) B_{ml} and (d) B_p) and normalized root mean squared values are given in Table 4.

Table 4: Fitting coefficients and associated normalized root mean squared error (*NRMSE*) values from for the *K* models shown in Figure 6. The coefficients for the models are given for fits to the data just for the homogeneous samples and for the fits to the data from all samples. The units for all values were converted to be consistent with the units used in this study.

	Homogeneous Clay Samples		All Samples					
Coefficients	Value	*NRMSE*	Value	*NRMSE*	Literature Values	Units	Equation	Figure
A_s	4.60×10^{-7}	0.301	4.76×10^{-7}	0.301	1.19×10^{-6} (a)	$mS^2/m/s$	11	6a
A_m	5.81×10^{-5}	0.424	4.93×10^{-5}	0.466	$9.55\text{x}10^{-5}$ (a)	$mS^2/m/s$	12	6b
B_{ml}	4.35×10^{-2}	0.0790	4.71×10^{-2}	0.0807	0.80-4.70 (b)	m/s^3	16	6c
B_p	3.49×10^{-2}	0.116	3.00×10^{-2}	0.104	0.80-4.70 (b)	m/s^3	16	6d

[a] Weller et al. (2015a); approximate value from their equation 27 and Figure 5b.

[b] Maurer and Knight (2016); average value given for borehole measurements in aquifer.

DISCUSSION

Our results demonstrate *K* is only well predicted from S_{por}, the proxy measure of clay content, and ϕ for the homogenous samples. The clustered clay content had a minimal impact on *K* over the range of clay contents, which results in a poor fit when equation 2 is used to model to the entire dataset. This result is expected as fluid should primarily flow through the hydraulically interconnected sand matrix between the clay clusters and S_{por} is not a good proxy for the inverse hydraulic radius in the clustered samples.

The SIP data are sensitive to changes in S_{por}, as both $\sigma''_{1\text{Hz}}$ and m_n vary with S_{por} (Figures 5a and 5b) regardless of clay distribution. The linear correlation between the SIP parameters and S_{por} has been extensively documented in the literature in homogeneous samples (e.g. Revil and

Florsch, 2010; Weller et al., 2010, Revil et al., 2017), but not in heterogeneous material, such as the clustered samples reported here. The primary difference between the homogeneous and clustered samples is that the coefficients C_s and C_m are higher for the homogeneous samples than for the clustered samples, which supports the results of Wildenschild et al. (2000) who observed higher DC surface conduction in their homogeneous clay mixtures compared to their clustered clay samples. This makes sense as in-phase surface conductivity is known to be proportional to the quadrature conductivity (Börner et al., 1996; Weller et al. 2013). Sugand (2015) also observed higher quadrature conductivity in their homogeneous samples compared to their clustered samples. Based on equations 6 and 10, clustered samples and homogeneous samples with similar clay content, mineralogy, fluid chemistry, and saturation should theoretically produce similar σ'' and m_n values. The decrease in these parameters for the clustered samples suggests there is a decrease in the electrical current density within the clay clusters. This indicates that the surface area available for polarization must be considered, where this “active surface area” is a function of the distribution of mineral grains in a porous medium.

In Figure 3d, we observe a clear and repeatable increase in signal amplitudes at frequencies lower than 1 Hz as a function of clay content. If the SIP measurement observes the clay clusters as very large, clay-coated grains experiencing EDL polarization, it is possible that a very low frequency (<0.01 Hz) peak would be associated with the clay clusters. Within the clusters, high clay content may lead to a reduction in the ionic mobility similar to what Weller et al. (2016) described for clay-bearing sandstones. These observations suggest that the active surfaces controlling the SIP spectra for the clustered clay samples may be isolated to the outer surfaces of the clusters. Tests at lower frequencies are necessary to confirm this hypothesis.

In the case of the homogeneous samples, the SIP data vary closely with K, especially when the 0% clay samples are removed. However, the SIP parameters for the clustered samples vary independently of K (Figures 6a and 6b). The non-negligible polarization of the clay clusters compromises the overall fit between the SIP parameters and K and suggests that the length scale controlling the SIP parameters may be more closely related to S_{por} than to the hydraulic radius in the sand-clay mixtures. Despite the polarization of the clay clusters, the SIP-K models (Figures 6a and 6b) still provide superior fits for both homogeneous and clustered clay sample data compared to the fits from the Kozeny-Carman equation (Figure 2). This suggests that the SIP active surface is a better proxy for the hydraulic radius than S_{por} in the tested samples.

Considering the NMR results, we find that the NMR relaxation times vary with S_{por} (Figures 5c and 5d) for homogeneous samples but only give moderately good *NRMSE* values. At high clay content (≥5%) it appears that relationship between T_{2ml} and S_{por} for the homogeneous samples may become linear, suggesting that S_{por} may be a better proxy for inverse pore size at higher clay content. However, at low clay content (<5%), the relationship appears nonlinear. This is likely because clay content variation at low clay contents (≤1%) will cause disproportionately large changes in surface area compared to pore size. These results demonstrate the potential pitfalls in applying T_{2ml} in equation 15 even in homogeneous sand-clay systems where S_{por} may not be an effective proxy for pore size. The relationship between T_{2p} and S_{por} in Figure 5d is non-linear, indicating that T_{2p} is not an appropriate measure of S_{por} in the tested range.

For the clustered samples, there is no linear relationship between the NMR parameters and S_{por}. This follows from examining the bimodal T_2 distributions in Figure 4b where the T_2

peak, controlled by the sand-bound pores dominates the T_2 distribution while S_{por} is primarily sensitive to the clay-bound surface area. This agrees with the results from Hinedi et al. (1997) who found that S_{por} in microporous silica beads was dominated by the microporosity that corresponded only to their fastest relaxation times. Further, our results support the findings of Stingaciu et al., (2009) who found that equation 15 could not be used to link the bimodal T_2 distributions to a bulk property like S_{por} in natural soils. It may instead be possible to represent the pore space more effectively using a weak-coupling relaxation model (Grunewald and Knight, 2009; Keating and Knight, 2012) to distinguish between S_{por} in sand-bound and clay-bound pore space. Ultimately, the NMR results in Figures 5c and 5d highlight the disconnect between the NMR T_2 distributions, which are sensitive to pore size distributions, and the bulk surface area measured by gas adsorption.

The distinct peaks in the clustered clay samples suggest there is little inter-pore coupling between the sand-bound water and the clay-bound water. We attribute this to the large size of the clay clusters, which reduce the probability that water molecules will diffuse through both clay- and sand-bound pores. This agrees with the findings of Grunewald and Knight (2009; 2011) who found that coarse heterogeneous sediments experienced less pore-coupling than fine-grained sediments. It is possible, however, that pore coupling would be observed in samples with smaller clay clusters or natural clay aggregates.

The fits between the NMR relaxation times and K (Figures 6c and 6d) are very good, consistently producing *NRMSE* values close to or less than 0.1 even when including the clustered sample data. The close fits show that the NMR parameters are better proxies of the hydraulic radius that controls K than that provided by S_{por} in the tested samples. However, care must be taken when applying this result broadly, as NMR is a measure of bulk properties and is insensitive to anisotropy. Taking the laminated clay systems studied by Anand et al., (2006) as an example, if the laminations were oriented orthogonal to the hydraulic gradient, the hydraulic radius would be controlled by the clay-bound porosity rather than the sand-bound porosity. This means the shorter T_2 peak would likely correspond to K. Since the T_2 distribution contains no directional information, it is impossible to know which T_2 peak contains the essential information about the hydraulic radius controlling K without additional information about pore connectivity. Thus, the non-uniqueness of the NMR response compromises its sensitivity to K in heterogeneous systems to a greater extent than our results indicate. Using pulsed-field gradient NMR methods to measure diffusional length scales (e.g. Latour et al., 1995) or combining the NMR measurements with additional measurements sensitive to anisotropy (e.g. SIP) may help to overcome this limitation.

The low variability in ϕ, ϕ_{NMR}, and F indicate that these parameters do not have a strong impact on the K models. Excluding these parameters from the K models in equations 2, 11, 12, and 16 results in similar fitting coefficients and *NRMSE* values. These results support the findings of Weller et al. (2015a), who found that F could be excluded from SIP-K models in unconsolidated materials, as well as the results of Maurer and Knight (2016), who showed that in unconsolidated aquifers that the n exponent in the SDR equation could be set to 0, negating the influence of ϕ_{NMR}. In unconsolidated systems with little pore space tortuosity, there appears to be no need to include ϕ, ϕ_{NMR}, or F in K-prediction models. A homogeneous, sandy system with low (<10%) clay content, such as the sand underlying the CFB Borden site in Canada (Sudicky and Illman, 2011), would likely satisfy these criteria.

We experimentally show that the sensitivity of SIP and NMR parameters to clay distribution in a sand matrix impacts the relationships between the physical and hydraulic parameters and the geophysical parameters. SIP parameters are linearly correlated to the clay content, with the correlation coefficient dependent on the clay distribution. The NMR relaxation time distributions are very sensitive to the distribution of pore sizes, resulting in very strong fits with K. As a result of their sensitivity to clay distribution, all geophysical parameters analyzed proved to be predictors of K rather than S_{por}, which is not sensitive to clay distribution. This suggests that geophysical methods may provide accurate field-scale estimates of K in heterogeneous geological environments where K models based on pore geometric parameters may be limited. Further study is necessary to understand the sensitivity of field SIP and NMR measurements to hydrogeological heterogeneity. This is particularly important for NMR measurements, which are only sensitive to bulk subsurface properties.

Future work should also focus on testing higher clay concentrations where the clusters may begin to impact K, different clay types expanding on the work of Anand et al. (2006) and Sugand (2015), and realistic geological analogs. The NMR results for the clustered samples in Figure 4b match closely with the laminated kaolinite samples from Anand et al. (2006), suggesting that they can be used to simulate systems where clay lenses are oriented parallel to the hydraulic gradient. However, further tests must be run to simulate a scenario where clay lenses are oriented orthogonally to the hydraulic gradient. Wildenschild et al. (2000) and Sugand (2015) have tested a small number of anisotropic sand-clay samples, observing that electrical measurements are sensitive to clay-lens orientation. Further tests on anisotropic clay distributions would provide an opportunity to better understand the sensitivity of SIP and NMR petrophysical models to anisotropy. Such studies would help develop geophysical *K* models that are robust to varying clay distribution in addition to content and type.

CONCLUSION

The quantity and distribution of kaolinite clay in synthetic sand-clay mixtures impacts the relationships between measured physical and hydraulic parameters and geophysical parameters. In homogeneous sand-clay samples, changes in clay content produce changes in hydraulic and geophysical parameters consistent with previous studies. When the clay is formed into large clusters, clay content no longer influences *K* and the geophysical responses become more complex. The SIP measurements are sensitive to increasing clay content as well as clay distribution and we find that the distribution of the clay controls the active surface area available for polarization. SIP estimates of *K* are overall superior to estimates from the Kozeny-Carman equation; however, variations in the SIP parameters in the clustered clay samples compromise the SIP-*K* models. The NMR T_2 distributions reflect the bimodal character of the pore space, with a second, short-time peak appearing with increasing clustered clay content. The characteristic NMR relaxation times do not closely track the increase in clay content but provide very accurate estimates of *K*, regardless of clay distribution. This suggests that the NMR parameters are more sensitive to the relevant hydraulic radius controlling *K* in these samples, compared to S_{por}, which is only sensitive for homogeneous samples. Further testing is required to understand how more geologically realistic clay distributions impact the relationships between *K* and the measured geophysical parameters.

Glossary: Definitions and units of all symbols used.

Symbol	Definition	Units
A	NMR signal amplitude	arb
A_0	NMR initial signal amplitude	arb
CEC	Cation exchange capacity	C/kg
f	Stern layer partition coefficient	-
F	Archie's electrical formation factor	-
f	Frequency	Hz
h	NMR signal fraction	-
k	Permeability	m^2
K	Hydraulic conductivity	m/s
m	Chargeability	-
m_n	Normalized chargeability	S/m
m_t	Total chargeability	-
$NRMSE$	Normalized root-mean square error	-
n	SDR porosity exponent	-
Q_s	Interfacial charge density at mineral surface	C/m^2
S_{por}	Pore volume-normalized surface area	1/µm
S_{SA}	Specific surface area	m^2/g
T_2	NMR transverse relaxation time	s
T_{2B}	NMR bulk water relaxation time	s
T_{2S}	NMR surface relaxation time	s
T_{2D}	NMR diffusion relaxation time	s
T_{2ml}	NMR mean-log relaxation time	s
T_{2p}	NMR relaxation time at T_2 distribution peak	s
V	Scaling factor between K and k	m*s
α	$\sigma''_{1Hz} \propto m_n$ proportionality constant	-
$\beta^S_{(+)}$	Ionic mobility in the Stern Layer	$m^2/s/V$
ϕ	Gravimetric porosity	(-)
ϕ_{NMR}	NMR-estimated porosity	(-)
ρ_g	Matrix density	g/m^2
σ^*	Complex electrical conductivity	S/m
σ'	Real electrical conductivity	S/m
σ''	Quadrature electrical conductivity	S/m
$\|\sigma\|$	Complex electrical conductivity magnitude	S/m
σ_0	Conductivity at zero frequency	S/m
σ_∞	Conductivity at high frequency asymptote	S/m
σ''_{1Hz}	Quadrature electrical conductivity at 1 Hz	S/m
σ_f	Conductivity of the saturating pore fluid	S/m
σ_s'	Real conductivity at the pore surface	S/m
θ	Complex conductivity phase angle	rad
τ	SIP relaxation time	s

Fitting Coefficients	Definition	Units
A_{KC}	Kozeny-Carman equation coefficient	$m/\mu m^2/s$
A_s/A_m	SIP-hydraulic conductivity model coefficient	$mS^2/m/s$
B_{ml}/B_p	SDR equation coefficient	m/s^3
C_s / C_m	SIP polarizability constant	mS um/m
ρ_{2ml}/ρ_{2p}	NMR surface relaxivity	m/s

APPENDIX A

Revil et al. (2017) define the following,

$$\sigma''=\frac{1}{F\phi}\frac{\lambda}{\alpha}\rho_g\mathrm{CEC}, \tag{A1}$$

$$m_n=\frac{1}{F\phi}\lambda\rho_g\mathrm{CEC}, \tag{A2}$$

$$\lambda=\beta^S_{(+)}f, \tag{A3}$$

Where α is a unitless proportionality constant between σ" and m_n, ρ_g is the grain density, the CEC is the cation exchange capacity (C/kg), $\beta^S_{(+)}$ is the ionic mobility of the counterions in the Stern Layer (m^2/s/V), and f is the partition coefficient describing the proportion of sorbed ions in the Stern Layer. Revil et al. (2013) defines the cation exchange capacity as:

$$\mathrm{CEC} = S_{sp}Q_s, \tag{A4}$$

where Q_s is the charge density at the mineral surface (C/m^2). Inserting A4 into equations A1 and A2 and combining with equation 1 gives the following expressions,

$$\sigma'' = \frac{\beta^S_{(+)}fQ_s}{\alpha}\frac{S_{por}}{F(1-\phi)}, \tag{A5}$$

$$m_n = \beta^S_{(+)}fQ_s\frac{S_{por}}{F(1-\phi)}, \tag{A6}$$

where we define,

$$C_s = \frac{\beta^S_{(+)}fQ_s}{\alpha}, \tag{A7}$$

$$C_m = \beta^S_{(+)} f Q_s. \tag{A8}$$

Using $\beta^S_{(+)}$ = 1.9×10^{-9} m^2/s/V, f = 0.98, Q_s = 0.32 C/m^2, and α = 8.1 (Revil et al., 2013; Revil et al., 2017), and converting to the appropriate units described in the Spectral Induced Polarization Theory subsection, we find that C_s = 7.35×10^{-2} mS/μm/m and C_m = 5.96×10^{-1} mS/μm/m.

REFERENCES

Archie, G., 1942, The electrical resistivity log as an aid in determining some reservoir characteristics: Transactions of the American Institute of Mining, Metallurgical, and Petroleum Engineers, **146**, 54–62.

Anand, V., G. J. Hirasaki, and M. Fleury, 2006, NMR diffusional coupling: effects of temperature and clay distribution, International Symposium of the Society of Core Analysts, doi: 10.1007/s00300-014-1595-6.

Anand, V., and G. J. Hirasaki, 2008, Paramagnetic relaxation in sandstones: distinguishing T1 and T2 dependence on surface relaxation, internal gradients and dependence on echo spacing: Journal of Magnetic Resonance, **190**, 68–85, doi:10.1016/j.jmr.2007.09.019.

Banavar, J. R., and L. M. Schwartz, 1987, Magnetic resonance as a probe of permeability in porous media: Physical Review Letters, **58**, 1411–1414, doi:10.1103/PhysRevLett.58.1411.

Bear, J., 1972, Dynamics of Fluids in Porous Media, Vol. 1: American Elsevier Publishing Company.

Behroozmand, A., K. Keating, and E. Auken, 2015, A review of the principles and applications of the NMR technique for near-surface characterization: Surveys in Geophysics, **36**, 27–85, doi:10.1007/s10712-014-9304-0.

Binley, A., S. S. Hubbard, J. A. Huisman, A. Revil, D. A. Robinson, K. Singha, and L. D. Slater, 2015, The emergence of hydrogeophysics for improved understanding of subsurface processes over multiple scales: Water Resources Research, **51**, 3837–3866, doi:10.1002/ 2015WR017016.

Börner, F. D. J. R. Schopper, and A. Weller, 1996, Evaluation of transport and storage properties in the soil and groundwater zone from induced polarization measurements: Geophysical Prospecting, **44**, 583–601. https://doi.org/10.1111/j.1365-2478.1996.tb00167.x

Brownstein, K. R., and C. E. Tarr, 1979, Importance of classical diffusion in NMR studies of water in biological cells: Physical Review A, **19**, 2446– 2453, doi: 10.1103/PhysRevA.19.2446.

Brunauer, S., P. H. Emmett, and E. Teller, 1938, Adsorption of gases in multimolecular layer: Journal of the American Chemical Society, **60**, 309–319, doi:10.1021/ja01269a023.

Bücker, M., and A. Hördt, 2013, Analytical modelling of membrane polarization with explicit parametrization of pore radii and the electrical double layer: Geophysical Journal International, **194**, 804–813, doi:10.1093/gji/ggt136.

Carman, P.C., 1939, Permeability of saturated sands, soils and clays: The Journal of Agricultural Science, **29**, 262-273. doi:10.1017/S0021859600051789.

Carrier, W. D., 2003, Goodbye, Hazen; Hello, Kozeny-Carman: Journal of Geotechnical and Geoenvironmental Engineering, **129**, 1054–1056, doi:10.1061/(ASCE)1090-0241(2003)129:11(1054).

Chapuis, R. P., and M. Aubertin, 2003, On the use of the Kozeny–Carman equation to predict the hydraulic conductivity of soils: Canadian Geotechnical Journal, **40**, 616–628, doi:10.1139/T03-013.

Coates, G. R., T. C. A. Peveraro, A. Hardwick, and D. Roberts, 1991, The magnetic resonance imaging log characterized by comparison with petrophysical properties and laboratory core data, paper presented at Society of Petroleum Engineers Annual Technical Conference and Exhibition.

Costabel, S., and U. Yaramanci, 2013, Estimation of water retention parameters from nuclear magnetic resonance relaxation time distributions: Water Resources Research, **49**, 2068–2079, doi:10.1002/wrcr.20207.

Daigle, H. and Dugan, B., 2009, Extending NMR data for permeability estimation in fine-grained sediments, Marine and Petroleum Geology, **26**, 1419–1427. doi: 10.1016/j.marpetgeo.2009.02.008.

Daigle, H. and Dugan, B., 2011, An improved technique for computing permeability from NMR measurements in mudstones, Journal of Geophysical Research: Solid Earth, **116**, 1–14, doi: 10.1029/2011JB008353.

Dlubac, K., R. Knight, Y. Q. Song, N. Bachman, B. Grau, J. Cannia, and J. Williams, 2013, Use of NMR logging to obtain estimates of hydraulic conductivity in the High Plains aquifer, Nebraska, USA: Water Resources Research, **49**, 1871–1886, doi:10.1002/wrcr.20151.

Dlugosch, R., T. Günther, M. Müller-Petke, and U. Yaramanci, 2013, Improved prediction of hydraulic conductivity for coarse-grained, unconsolidated material from nuclear magnetic resonance: Geophysics, **78**, EN55-EN64, doi:10.1190/geo2012-0187.1.

Domenico, P. A., and F. W. Schwartz, 1990, Physical and Chemical Hydrogeology: John Wiley.

Foley, I., S. Farooqui, and R. Kleinberg, 1996, Effect of Paramagnetic Ions on NMR Relaxation of Fluids at Solid Surfaces: Journal of Magnetic Resonance A, **123**, 95–104, doi:10.1006/jmra.1996.0218.

Grunewald, E., and R Knight, 2009, A Laboratory Study of NMR Relaxation Times and Pore Coupling in Heterogeneous Media: Geophysics, **74**, E215, doi: 10.1190/1.3223712.

Grunewald, E., and R. Knight, 2011, A laboratory study of NMR relaxation times in unconsolidated heterogeneous sediments. Geophysics, **76**, G73–G83, doi: 10.1190/1.3581094.

Godefroy, S., J.-P. Korb, M. Fleury, and R. & Bryant, 2001, Surface nuclear magnetic relaxation and dynamics of water and oil in macroporous media: Physical Review E, **64**, 21605, doi: 10.1103/PhysRevE.64.021605.

Hinedi, Z. R., A. C. Chang, M. A. Anderson, and D. B. Borchardt, 1997, Quantification of microporosity by nuclear magnetic resonance relaxation of water imbibed in porous media, Water Resources Research, **33,** 2697–2704, doi: 10.1029/97WR02408.

Howard J., and W. Kenyon, 1992, Determination of pore size distribution in sedimentary rocks by proton nuclear magnetic resonance. Marine and Petroleum Geology, **9**, 139-145, doi: 10.1016/0264-8172(92)90086-T.

Johnson, D., J. Koplik, and L. Schwartz, 1986, New pore-size parameter characterizing transport in porous media: Physical Review Letters, **57**, 2564–2567, doi: 10.1103/PhysRevLett.57.2564.

Keating, K., and R. Knight, 2007, A laboratory study to determine the effect of iron oxides on proton NMR measurements: Geophysics, **72**, E27–E32, doi:10.1190/1.2399445.

Keating, K., R. Knight, 2012, The effect of spatial variation in surface relaxivity on nuclear magnetic resonance relaxation rates: Geophysics, **77**, E365–E377, https://doi.org/10.1190/geo2011-0462.1.

Keating, K., 2014, A laboratory study to determine the effect of surface area and bead diameter on NMR relaxation rates of glass bead packs: Near Surface Geophysics, **12**, 243–254, doi:10.3997/1873-0604.2013064.

Keery, J., A. Binley, A. Elshenawy, and J. Clifford, 2012, Markov-chain Monte Carlo estimation of distributed Debye relaxations in spectral induced polarization: Geophysics, **77**, E159, doi:10.1190/geo2011-0244.1.

Keller, C. K., G. Van Der Kamp, and J. A. Cherry, 1989, A multiscale study of the permeability of a thick clayey till: Water Resources, **25**, 2299–2317, doi:10.1029/WR025i011p02299.

Kemna, A., A. Binley, C. Giorgio, E. Niederleithinger, A. Revil, L. Slater, K. H. Williams, A. F. Orozco, F. Haegel, A. Hördt, S. Kruschwitz, V. Leroux, K. Titov, E. Zimmermann., 2012, An overview of the spectral induced polarization method for near-surface applications: Near Surface Geophysics, **10**, 453–468, doi:10.3997/1873-0604.2012027.

Kenyon W., R. Kleinberg, C. Straley, 1995, Nuclear Magnetic Resonance Imaging: Technology for the 21st Century. Oilfield Review, **7**, 19-33.

Kleinberg, R. L., 1996, Utility of NMR T_2 distributions, connection with capillary pressure, clay effect, and determination of the surface relaxivity parameter ρ_2: Magnetic Resonance Imaging, **14**, 761–767.

Kleinberg, R. L., and M. A. Horsfield, 1990, Transverse relaxation processes in porous sedimentary rock: Journal of Magnetic Resonance, **88**, 9–19, doi:10.1016/0022-2364(90)90104-H.

Latour, L. L., R. L. Kleinberg, P. P. Mitra, and C. H. Sotak, 1995, Pore-size distributions and tortuosity in heterogeneous porous media, Journal of Magnetic Resonance, Series A, **112,** 83-91, doi: 10.1006/jmra.1995.1012.

Leroy, P., A. Revil, Kemna, P. Cosenza, and A. Ghorbani, 2008, Complex conductivity of water-saturated packs of glass beads: Journal of Colloid Interface Science, **321**, 103–17, doi: 10.1016/j.jcis.2007.12.031.

Marshall, D. J., and T. R. Madden, 1959, Induced polarization, a study of its causes: Geophysics, **24**, 790–816, doi:10.1190/1.1438659.

Maurer, J., and R. Knight, 2016, Models and methods for predicting hydraulic conductivity in near-surface unconsolidated sediments using nuclear magnetic resonance: Geophysics, **81**, D503–D518, doi:10.1190/geo2015-0515.1.

Meiboom, S., and D. Gill, 1958, Modified spin-echo method for measuring nuclear relaxation times: The Review of Scientific Instruments, **29**, 688–691, doi:10.1063/1.1716296.

Minagawa, H., Y. Nishikawa, I. Ikeda, K. Miyazaki, N. Takahara, Y. Sakamoto, T. Komai, and H. Narita, 2008, Characterization of sand sediment by pore size distribution and permeability using proton nuclear magnetic resonance measurement: Journal of Geophysical Research, **113**, B07210, doi:10.1029/2007JB005403.

Moss, A., and X. Jing, 2001, An investigation into the effect of clay type, volume and distribution on NMR measurements in sandstones, Society of Core Analysts Symposium.

Morriss, C., D. Rossini, C. Straley, P. Tutunjian, and H. Vinegar, 1997, Core analysis by low-field NMR, *The Log Analyst*, **38**.

Neuzil, C. E., 1986, Groundwater Flow in Low-Permeability Environments: Water Resources Research, **22**, 1163–1195, doi:10.1029/WR022i008p01163.

Nordsiek, S., and A. Weller, 2008, A new approach to fitting induced-polarization spectra: Geophysics, **73**, F235–F245, doi:10.1190/1.2987412.

Nordsiek, S., E. Diamantopoulos, A. Hördt, and W. Durner, 2016, Relationships between soil hydraulic parameters and induced polarization spectra: Near Surface Geophysics, **14**, 23–37, doi:10.3997/1873-0604.2015050.

Ntarlagiannis, D. and L. Slater, 2014, Quantifying the Accuracy of Laboratory SIP Experimental Set Ups: Presented at the 2014 Fall Meeting, AGU.

Okay, G., P. Leroy, A. Ghorbani, P. Cosenza, C. Camerlynck, J. Cabrera, N. Florsch, and A. Revil, 2014, Spectral induced polarization of clay-sand mixtures: Experiments and modeling: Geophysics, **79**, E353–E375, doi:10.1190/geo2013-0347.1.

Osterman, G., K. Keating, A. Binley, and L. D. Slater, 2016, A laboratory study to estimate pore geometric parameters of sandstones using complex conductivity and nuclear magnetic resonance for permeability prediction: Water Resources Research, **52**, 4321–4337, doi:10.1002/2015WR018472.

Ozgumus, T., M. Mobedi, and U. Ozkol, 2014, Determination of Kozeny constant based on porosity and pore to throat size ratio in porous medium with rectangular rods: Engineering Applications of Computational Fluid Mechanics, **52**, 308-318, doi:10.1080/19942060.2014.11015516.

Palacky, G. J., 1987, Clay mapping using electromagnetic methods: First Break, **5**, 295-306, doi: 10.3997/1365-2397.1987015.

Pape, H., L. Riepe, and J. R. Schopper, 1987, Interlayer conductivity of rocks - a fractal model of interface irregularities for calculating interlayer conductivity of natural porous mineral systems: Colloids and Surfaces, **27**, 97–122, doi:10.1016/0166-6622(87)80331-1.

Revil, A., and L. M. Cathles, 1999, Permeability of shaly sands: Water Resources Research, **35**, 651–662, doi:10.1029/98WR02700.

Revil, A., and N. Florsch, 2010, Determination of permeability from spectral induced polarization in granular media: Geophysical Journal International, **181**, 1480–1498, doi:10.1111/j.1365-246X.2010.04573.x.

Revil, A., 2012, Spectral induced polarization of shaly sands: Influence of the electrical double layer: Water Resources Research, **48** W02517, doi: 10.1029/2011WR011260.

Revil, A., 2013, On charge accumulation in heterogeneous porous rocks under the influence of an external electric field: Geophysics, **78**, D271–D291, doi:10.1190/geo2012-0503.1.

Revil, A., J. D. Eppehimer, M. Skold, M. Karaoulis, L. Godinez, and M. Prasad, 2013, Low-frequency complex conductivity of sandy and clayey materials. Journal of Colloid and Interface Science, **398**, 193–209, doi:10.1016/j.jcis.2013.01.015.

Revil, A., A. Binley, L. Mejus, and P. Kessouri, 2015, Predicting permeability from the characteristic relaxation time and intrinsic formation factor of complex conductivity spectra, Water Resources Research, **51**, 6672–6700, doi:10.1002/2015WR017074.

Revil, A., A. Coperey, A. Shao, N. Florsch, I. L. Fabricius., Y. Deng, J. R. Delsman, P. S. Pauw, M. Karaoulis, P. G. B. de Louw, E.S. van Baaren, W. Dabekaussen, A. Menkovic, and J. L. Gunnink, 2017, Complex conductivity in soils: Water Resources Research, **53**, 5121-7147, doi: 10.1002/2017WR020655.

Ryu, S., 2009, Effect of inhomogeneous surface relaxivity, pore geometry and internal field gradients on NMR logging: Exact and perturbative theories and numerical investigations: presented at SPWLA 50th Annual Logging Symposium.

Seevers, D. O., 1966, A nuclear magnetic method for determining the permeability of sandstones, 7th Annual Logging Symposium: presented at Society of Petrophysical Well Log Analysts.

Sen, P. N., P. A. Goode, and A. Sibbit, 1988, Electrical conduction in clay bearing sandstones at low and high salinities: Journal of Applied Physics, **63**, pp.4832-4840, doi: 10.1063/1.340476.

Slater, L. D., and D. R. Glaser, 2003, Controls on induced polarization in sandy unconsolidated sediments and application to aquifer characterization: Geophysics, **68**, 1547–1558, doi:10.1190/1.1620628.

Slater, L., D. Ntarlagiannis, and D. Wishart, 2006, On the relationship between induced polarization and surface area in metal-sand and clay-sand mixtures: Geophysics, **71**, A1–A5, doi:10.1190/1.2187707.

Slater, L., 2007, Near surface electrical characterization of hydraulic conductivity: from petrophysical properties to aquifer geometries—a review: Surveys in Geophysics, **28**, 169–197, doi:10.1007/s10712-007-9022-y.

Stingaciu, L. R., A. Pohlmeier, P. Blümler, L. Weihermüller, D. van Dusschoten, S. Stapf, and H. Vereecken, 2009, Characterization of unsaturated porous media by high-field and low-field NMR relaxometry: Water Resources Research., **45**, W08412, doi:10.1029/2008WR007459.

Sudicky, E. A., and W. A. Illman, 2011, Lessons learned from a suite of CFB Borden experiments. Groundwater, **49**, 630–48, doi.org/10.1111/j.1745-6584.2011.00843.x.

Sugand M. G., 2015, Effect of microstructural variation on hydrogeophysical properties of unconsolidated sand – clay mixtures: M.S. thesis, Lancaster University.

Swanson, R. D., A. Binley, K. Keating, S. France, G. Osterman, F. D. Day-Lewis, and K. Singha, 2015, Anomalous solute transport in saturated porous media: relating transport model parameters to electrical and nuclear magnetic resonance properties, Water Resources Research, **51**, 1264–1283, doi: 10.1002/2014WR015284

Sumner, J. S., 1976, Principles of induced polarization for geophysical exploration: Elsevier, New York, NY.

Timur, A., 1969, Pulsed nuclear magnetic resonance studies of porosity, movable fluid, and permeability of sandstones: Society of Petroleum Engineers, 21, 775-786, doi:10.2118/2045-PA.

Titov, K., V. Komarov, V. Tarasov, and A. Levitski, 2002, Theoretical and experimental study of time domain-induced polarization in water-saturated sands: Journal of Applied Geophysics, **50**, 417–433, doi:10.1016/S0926-9851(02)00168-4.

Vinegar, H. J., and M. H. Waxman, 1984, Induced polarization of shaly sands: Geophysics, **49**, 1267–1287, doi:10.1190/1.1441755.

Wallace, D. W., 2015, A laboratory study to develop a permeability model for unconsolidated glass bead packs by combining NMR and SIP measured parameters: M.S. thesis, Rutgers University-Newark.

Weller, A., L. Slater, S. Nordsiek, and D. Ntarlagiannis, 2010, On the estimation of specific surface per unit pore volume from induced polarization: a robust empirical relation fits multiple data sets: Geophysics, **75**, WA105–WA112. doi:10.1190/1.3471577.

Weller, A.; Breede, K.; Slater, L.; Nordsiek, S. 2011, Effect of changing water salinity on complex conductivity spectra: Geophysics **76**, No. 6, F315-F327, doi: 10.1190/GEO2011-0072.1

Weller, A., L. Slater, and S. Nordsiek, 2013, On the relationship between induced polarization and surface conductivity: implications for petrophysical interpretation of electrical measurements: Geophysics, **78**, D315–325, doi:10.1190/geo2013-0076.

Weller and Slater, 2015, Induced polarization dependence on pore space geometry: Empirical observations and mechanistic predictions: Journal of Applied Geophysics, **123**, 310-315, doi: 10.1016/j.jappgeo.2015.09.002.

Weller, A., L. Slater, A. Binley, S. Nordsiek, and S. Xu, 2015a, Permeability prediction based on induced polarization: Insights from measurements on sandstone and unconsolidated samples spanning a wide permeability range: Geophysics, **80**, D161–D173, doi:10.1190/GEO2014-0368.1.

Weller, A.; L. Slater, J. A. Huisman, O. Esser, F.-H. Haegel, 2015b, On the specific polarizability of sands and sand-clay mixtures. Geophysics **80**, A57-A61, doi: 10.1190/geo2014-0509.1.

Whittall, K. P., M. J. Bronskill, and R. M. Henkelman, 1991, Investigation of analysis techniques for complicated NMR relaxation data: Journal of Magnetic Resonance, **95**, 221–234, doi:10.1016/0022-2364(91)90213-D.

Wildenschild, D., J. J. Roberts, and E. D. Carlberg, 2000, On the relationship between microstructure and electrical and hydraulic properties of sand-clay mixtures: Geophysical Research Letters, **27**, 3085–3088, doi:10.1029/2000GL011553.

Zisser, N., A. Kemna, and G. Nover, 2010, Relationship between low-frequency electrical properties and hydraulic permeability of low-permeability sandstones: Geophysics, **75**, E131–E141, doi:10.1190/1.3413260.

LIST OF FIGURES

Figure 1: Examples of dry samples prior to packing, (a) 90% sand mixed homogeneously with 10% clay; (b) 90% sand mixed with 10% clay clustered in ~5 mm balls; (c) clay clusters shown with a US quarter for scale.

Figure 2: K versus ϕ/S_{por}^2 for all samples. The dashed line and dotted lines show the fit of Equation 2 to the homogeneous data and the entire dataset, respectively. The coefficients, (A_{KC}), and normalized root mean squared values are given in Table 2.

Figure 3: SIP data collected for representative homogeneous and clustered samples for each clay content (samples H00A, H01A, H05A, and H10A shown in (a) and (c); samples H00A C01A, C05A, and C10A shown in (b) and (d)). SIP σ' spectra for (a) homogeneous samples and (b) clustered samples and SIP σ'' spectra for (c) homogeneous samples and (d) clustered samples.

Figure 4: NMR T_2 distributions for representative (a) homogenous samples and (b) clustered samples from each clay content (samples H00A, H01A, H05A, and H10A shown in (a); samples H00A C01A, C05A, and C10A shown in (b).

Figure 5: Characteristic geophysical parameters plotted versus pore geometric parameters: SIP parameters σ''_{1Hz} (a) and m_n (b) versus $S_{por}/[F(1-\phi)]$; NMR parameters $1/T_{2ml}$ (c) and $1/T_{2p}$ (d)

versus S_{por}. The dashed line shows the line of best fit for the data from the homogeneous samples; the dot-dashed lines shows the line of best fit for the clustered samples, given by (a) equation 6, (b) equation 10, and (c-d) equation 15. The coefficients C_s (a), C_m (b), ρ_{2ml} (c), and ρ_{2p} (d) were determined from fitting the $\log_{10}$ parameters in a least-squared sense and are given along with the corresponding normalized root mean squared values in Table 3.

Figure 6: Geophysical parameters plotted against K: SIP parameters $1/F\left[\sigma''_{1\mathrm{Hz}}\right]^2$ (a) and $1/F\ m_n^2$ (b); NMR parameters $\phi_{NMR}^4 T_{2ml}^2$ (c) and $\phi_{NMR}^4 T_{2p}^2$ (d). The dashed line and dotted lines show fitted K-models for the homogeneous data and the entire dataset, respectively, given by (a) equation 11, (b) equation 12, and (c-d) equation 16. The coefficients ((a) A_s, (b) A_m, (c) B_{ml} and (d) B_p) and normalized root mean squared values are given in Table 4.

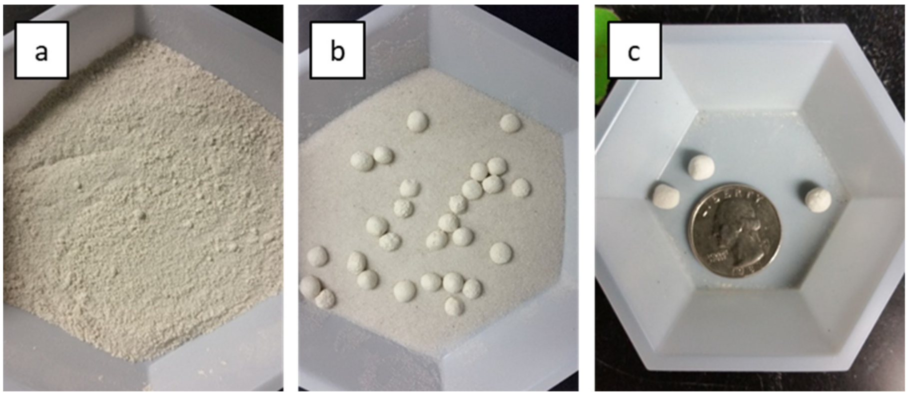

Figure 1

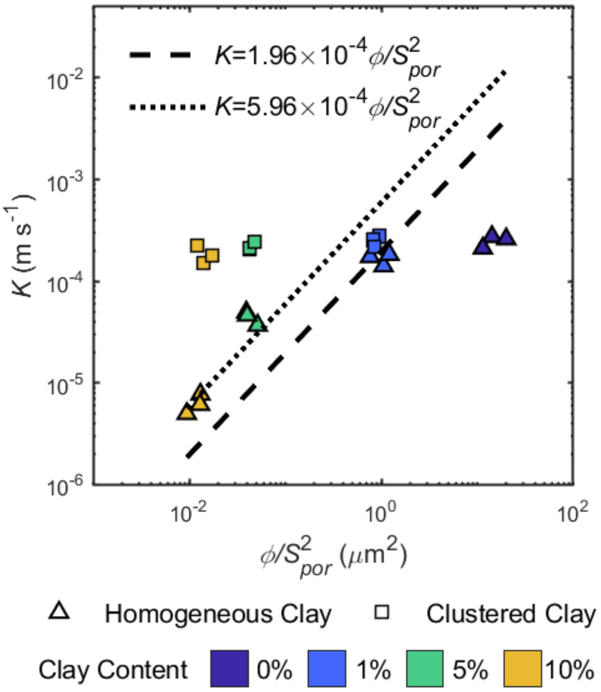
K=1.96×10^-4 φ/S^2_por
K=5.96×10^-4 φ/S^2_por
10^-2
10^-3
10^-4
10^-5
10^-6
K (m s^-1)
10^-2
10^0
10^2
φ/S^2_por (μm^2)
△ Homogeneous Clay
□ Clustered Clay
Clay Content
0%
1%
5%
10%

Figure 2

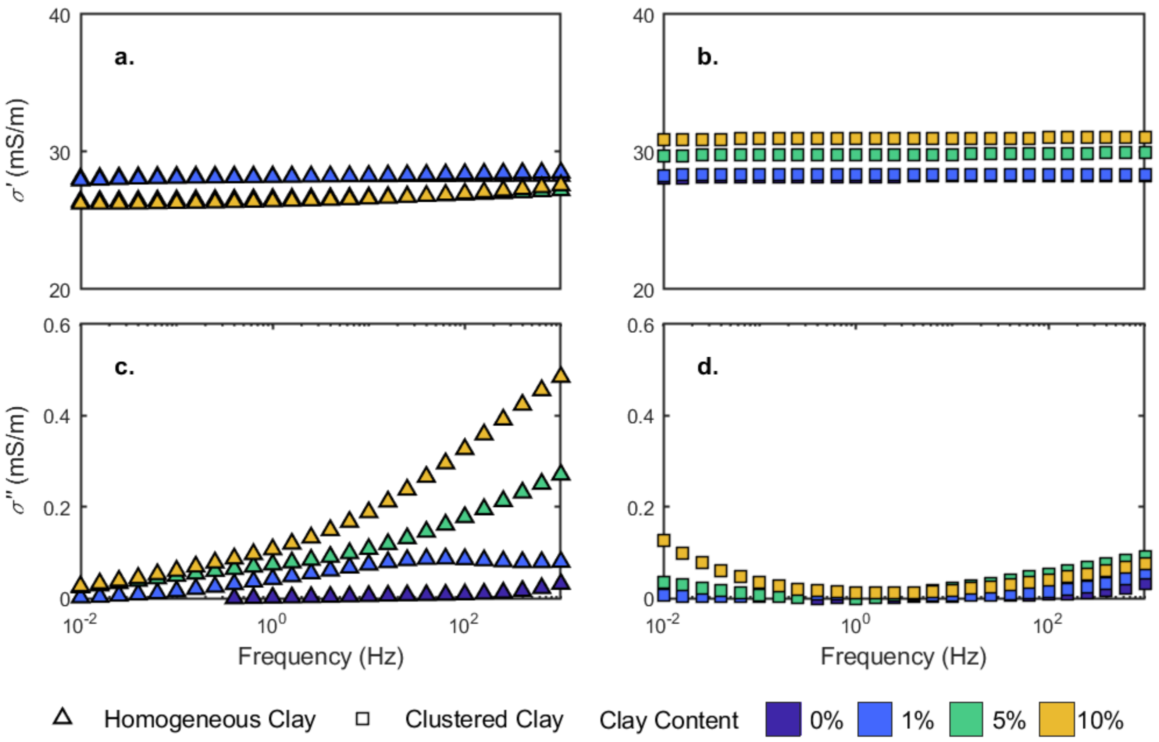
a.
b.
c.
d.
σ' (mS/m)
σ'' (mS/m)
40
30
20
0.6
0.4
0.2
0
10^{-2}
10^{0}
10^{2}
Frequency (Hz)
Homogeneous Clay
Clustered Clay
Clay Content
0%
1%
5%
10%

1

2 Figure 3

3

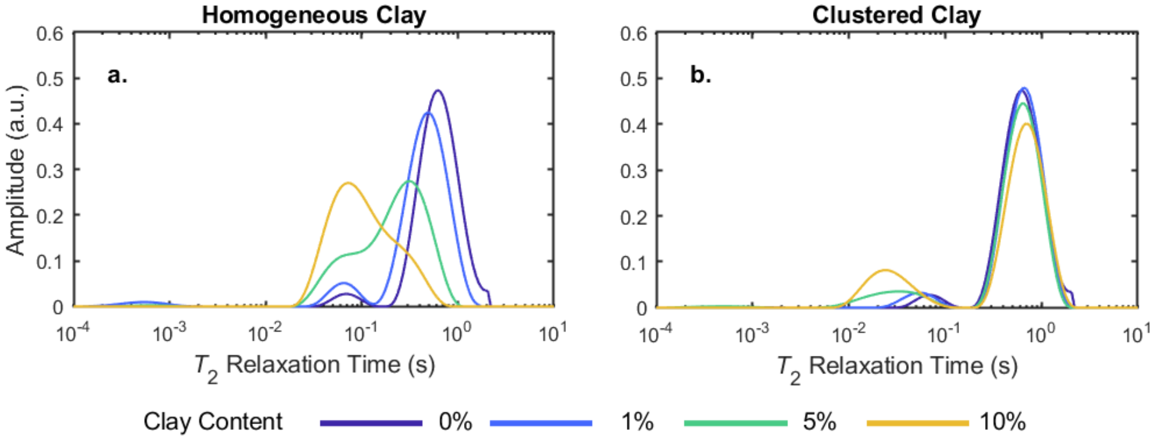
Homogeneous Clay
Clustered Clay
a.
b.
Amplitude (a.u.)
0.6
0.5
0.4
0.3
0.2
0.1
0
10^{-4}
10^{-3}
10^{-2}
10^{-1}
10^{0}
10^{1}
T_2 Relaxation Time (s)
Clay Content
0%
1%
5%
10%

Figure 4

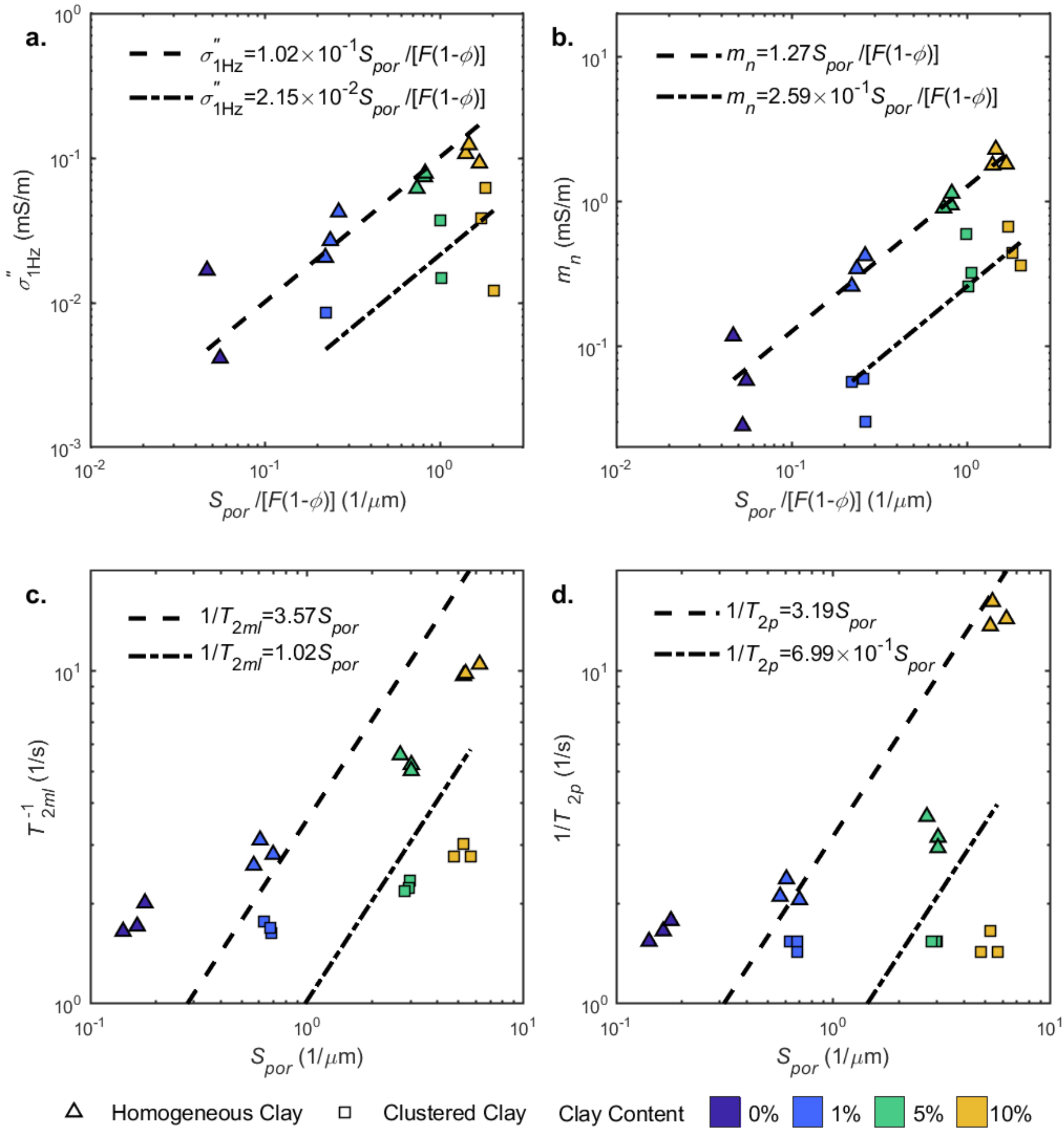
a.
$\sigma''_{1Hz}=1.02\times10^{-1}S_{por}/[F(1-\phi)]$
$\sigma''_{1Hz}=2.15\times10^{-2}S_{por}/[F(1-\phi)]$
σ''_{1Hz} (mS/m)
$S_{por}/[F(1-\phi)]$ (1/μm)
10^{0}
10^{-1}
10^{-2}
10^{-3}
b.
$m_n=1.27S_{por}/[F(1-\phi)]$
$m_n=2.59\times10^{-1}S_{por}/[F(1-\phi)]$
m_n (mS/m)
$S_{por}/[F(1-\phi)]$ (1/μm)
10^{1}
c.
$1/T_{2ml}=3.57S_{por}$
$1/T_{2ml}=1.02S_{por}$
T^{-1}_{2ml} (1/s)
S_{por} (1/μm)
d.
$1/T_{2p}=3.19S_{por}$
$1/T_{2p}=6.99\times10^{-1}S_{por}$
$1/T_{2p}$ (1/s)
S_{por} (1/μm)
△ Homogeneous Clay
□ Clustered Clay
Clay Content
0%
1%
5%
10%

Figure 5

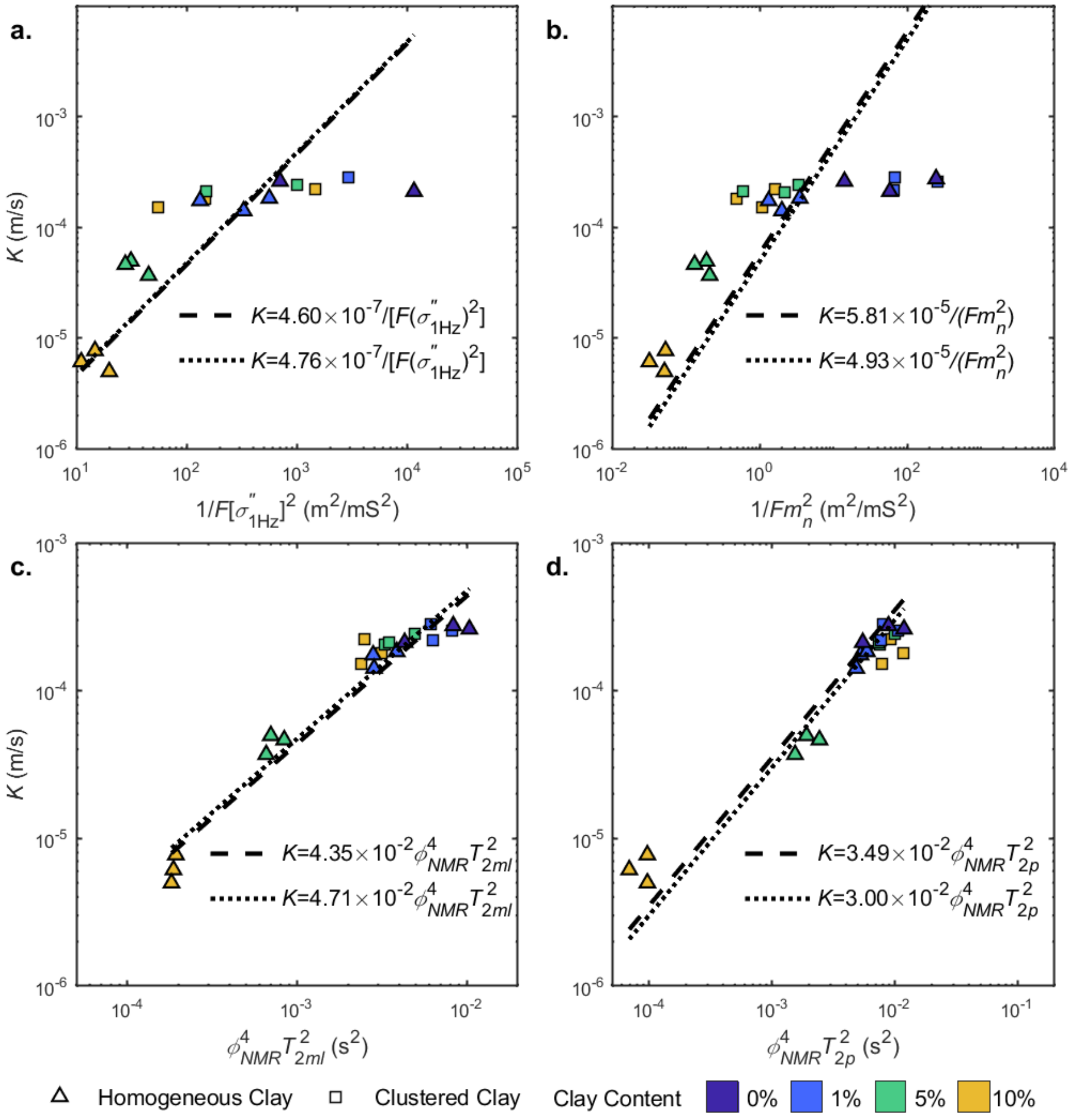
a.
b.
c.
d.
K (m/s)
10^{-3}
10^{-4}
10^{-5}
10^{-6}
K=4.60×10^{-7}/[F(σ''_{1Hz})^2]
K=4.76×10^{-7}/[F(σ''_{1Hz})^2]
10^1 10^2 10^3 10^4 10^5
1/F[σ''_{1Hz}]^2 (m^2/mS^2)
K=5.81×10^{-5}/(Fm_n^2)
K=4.93×10^{-5}/(Fm_n^2)
10^{-2} 10^0 10^2 10^4
1/Fm_n^2 (m^2/mS^2)
K=4.35×10^{-2}$\phi^4_{NMR}T^2_{2ml}$
K=4.71×10^{-2}$\phi^4_{NMR}T^2_{2ml}$
10^{-4} 10^{-3} 10^{-2}
$\phi^4_{NMR}T^2_{2ml}$ (s^2)
K=3.49×10^{-2}$\phi^4_{NMR}T^2_{2p}$
K=3.00×10^{-2}$\phi^4_{NMR}T^2_{2p}$
10^{-4} 10^{-3} 10^{-2} 10^{-1}
$\phi^4_{NMR}T^2_{2p}$ (s^2)
△ Homogeneous Clay
□ Clustered Clay
Clay Content
0%
1%
5%
10%

Figure 6